UPPSALA
UNIVERSITET

UPTEC K 20027
Examensarbete 30 hp
Augusti 2020

Nanocellulose surface functionalization for in-situ growth of zeolitic imidazolate framework 67 and 8

Beyar Abdulla

UPPSALA
UNIVERSITET

Teknisk- naturvetenskaplig fakultet
UTH-enheten

Besöksadress:
Ångströmlaboratoriet
Lägerhyddsvägen 1
Hus 4, Plan 0

Postadress:
Box 536
751 21 Uppsala

Telefon:
018 – 471 30 03

Telefax:
018 – 471 30 00

Hemsida:
http://www.teknat.uu.se/student

Abstract

Nanocellulose surface functionalization for in-situ growth of zeolitic imidazolate framework-67 and 8

Beyar Abdulla

This master's thesis was conducted at the Department of Nanotechnology and Functional Materials at Ångström Laboratory as part of an on-going project to develop hybrid nanocomposites from Cladophora cellulose and a sub-type of metal-organic frameworks; zeolitic imidazolate frameworks (ZIFs).
By utilizing a state-of-the-art interfacial synthesis approach, in-situ growth of ZIF particles on the cellulose could be achieved. TEMPO-mediated oxidation was diligently used to achieve cellulose nanofibers with carboxylate groups on their surfaces. These were ion-exchanged to promote growth of ZIF particles in a nanocellulose solution and lastly, metal ions and organic linkers which the ZIFs are composed of were added to the surface functionalized and ion-exchanged nanocellulose solution to promote ZIF growth. By vacuum filtration, mechanical pressing and furnace drying; freestanding nanopapers were obtained. A core-shell morphology between the nanocellulose and ZIF crystals was desired and by adjusting the metal ion concentration, a change in morphologies was expected. The nanocomposites were investigated with several relevant analytical tools to confirm presence, attachment and in-situ growth of ZIF crystal particles upon the surface of the fine nanocellulose fibers.
Both the CNF@ZIF-67 and CNF@ZIF-8 nanocomposites were successfully prepared as nanopapers with superior surface areas and thermal properties compared to pure TEMPO-oxidized cellulose nanopapers. The CNF@ZIFs showcased hierarchical porosities, stemming from the micro- and mesoporous ZIFs and nanocellulose, respectively. Also, it was demonstrated that CNF@ZIF-8 selectively adsorbed CO_2 over N_2. Partial formation of core-shell structure could be obtained, although a relationship between increased metal ions and ZIF particle morphology could not wholly be observed.

Handledare: Chao Xu
Ämnesgranskare: Maria Strømme
Examinator: Peter Broqvist
ISSN: 1650-8297, UPTEC K 20027
Tryckt av: UPPSALA

Populärvetenskaplig sammanfattning

Under många år har mänskligheten och vår natur utsatts för industrirelaterade utsläpp. Allt eftersom industrin växer, kommer dessa utsläpp att öka i mängd och enligt WHO befann vi oss, under 2018, i ett stadium där ca 90% av all världens population andades förorenad luft till viss mån.

För att motverka dessa utsläpp och minimera mängden giftiga gaser, såsom CO_2, har man flitigt varit på jakt efter material och produkter vilka skulle kunna implementeras inom industriella områden. Detta bidrar alltså till att b.la. etablerade produktionsmetoder blir mer hållbara för framtiden eller att nya produkter skapas för att ersätta befintlig teknologi inom separering, lagring eller omvandling av miljöfarliga utsläpp. Exempelvis används s.k. zeoliter flitigt inom industriella sammanhang. Dessa material är uppbyggda av aluminat (AlO_4) och silikat (SiO_4), vilka agerar byggstenar som bundna tillsammans bidrar till skapandet av ett enda stort, öppet nätverk av mikroporer. Denna struktur möjliggör att materialet kan agera som b.la. molekylsikt för selektiv separering av gaser. Sedan 2019 har det skapats ca. 235 typer av zeoliter för olika sammanhang, varvid många av dessa förekommer naturligt. Däremot finns det fortfarande begränsningar i hur man kan manipulera zeoliter för att erhålla nya strukturer vid syntes, för olika applikationer.

En relativt ny klass av porösa material som uppmärksammats under senaste åren är *metall-organiska* material (*metal-organic frameworks* eller MOFs på engelska). Dessa material besitter mycket stor ytarea och har inom forskningen diskuterats som användbara inom industrin för diverse applikationer. Exempelvis har de konstaterats kunna användas som lagringsmaterial för gaser eller som katalysatorer. Generellt består dessa utav metalljoner som koordinerar med organiska ligander och bildar ett kristallint, mikroporöst nätverk. Möjligheten till att använda olika kombinationer av metalljoner och organiska ligander har bidragit till att över 6000 MOFs syntetiseras årligen sedan dess upptäckt. På laborativ skala erbjuds en kontrollerad process som öppnar upp möjligheten för en skräddarsydd syntetisering av ett material med olika egenskaper som exempelvis optimal katalytisk förmåga, selektiv separering av gaser eller infoga elektrokemiska egenskaper i MOF:en. En begränsning som hindrar materialet från industriell tillämpning är dess mekaniska egenskaper, mer specifikt dess höga grad av sprödhet.

För att gynna MOF:ens implementering inom industrin har man försökt kombinera dessa med ett annat material via nanoteknologiska engagemang. Exempelvis kan man utnyttja ett polymert substrat som man inkorporerar MOF partiklar i för att bilda flexibla nanokompositer som erhåller det bästa av två världar. Problemet har dock dels varit att MOF-partiklarna endast fysiskt är inblandade i kompositen och att polymererna har petrokemiska ursprung, vilket dessvärre bidrar till miljöbelastning. Däremot har ny forskning visat att biopolymerer skulle kunna vara goda kandidater som substratmaterial.

I detta projekt användes en gränsskiktssyntes i lösning för att skapa en nanokomposit genom att växa en sub-typ av MOF (*zeolitic imidazolate frameworks* eller s.k. ZIFs) på cellulosa från en grön alg, *Cladophora*. Metoden gick ut på att introducera funktionella grupper på cellulosan och samtidigt defibrillera den till fina nanofibrer (TEMPO-CNFs) via en kemisk metod, s.k. TEMPO-oxidering. Dessa funktionella grupper kunde sedan agera som aktiva säten på vilka ZIF- partiklar

kunde fästa sig vid och växa till nanopartiklar i en lösning. Lösningen filtrerades och kvar erhöll man ett flexibelt papper bestående av en nanokomposit som benämndes CNF@ZIFs. Syftet var att undersöka huruvida ZIF kristallernas morfologi på cellulosafibrerna kunde manipuleras genom att ändra koncentrationen metalljoner i lösningen för att gynna skapandet av ZIF-lager istället för individuella nanopartiklar.

Contents

Acknowledgement

I would like to thank my subject reader; Professor Maria Strømme for allowing me to perform my masters thesis at the Department of Nanotechnology and Functional materials in Uppsala University, Ångströms laboratory.

My project supervisor, Dr. Chao Xu, had his door always open for me whenever I had questions or doubts regarding specific matters related to the project. Your passion and ambition were infectious and discussions with you were always insightful. Secondly, Shengyang Zhou and Xueying Kong; Thank you both for being there for me during laborations and if I had questions regarding the report. Shengyang your energy and positive attitude was very uplifting. Xueying, I am very grateful for your help preparing my samples prior the SEM imaging. Both of you are very bright minds and you always made me feel as if I was a part of the team.

To my beloved parents (Jowan Hafeed and Parosh Aziz Abdulla), sister (Yara Abdulla), cousins (Miran- and Mandy Aziz and little Josef Mohammed), aunts (Naza- and Chra Hafeed), grandparents (Farok- and Akhter Hafeed); You have always been an integral part of my life and this journey was certainly not an exception. My love for all of you is unconditional.

To my friends, Andreas Abdelki and Mikael Svensson which were doing their respective thesis works at the department too; I am glad and thankful to have had you guys by my side throughout my thesis work. The discussions we had were always fruitful and the mental support you two gave me was very encouraging. Andreas, your kind and supportive nature towards me is beyond measure. Thank you for being you. Mikael, your thoughtful words and ability to carefully listen to my thoughts are admirable traits.

Lastly, to all the fellow workers at the department; I wish you well and good luck with your respective researches!

1. Introduction

1.1 Background

Our modern world is in strong symbiosis with the technological industry, which provides us with a high quality of life. Although, as our demands grow and technology always has to keep up, our environment suffers due to inevitable emissions and pollution from the expansion of our industries. Striving for a more sustainable future by addressing and trying to resolve issues such as environmental degradation from emissions has been a collective aim of humankind for many years. For instance, according to a report by the World Health Organization (WHO), as of 2018 nearly 90% of the human population unfortunately breathes polluted air to some degree [1]. Much effort has been put into trying to resolve the impact that the environment and humans have had to endure from emissions, such as carbon dioxide from usage of fossil fuels. Such advances within the field, as an example, is using porous materials as suitable receptors to encapsulate and /or diminish the toxicity of pollutants.

Porous materials, especially as we tread down on the nanoscale, have the intrinsic property of retaining high surface areas due to the presence of small voids which occur throughout the structure, on micro- and nanoscale. Examples of porous materials which have been used commercially are zeolites. These materials are composed of aluminosilicates and retain large surface areas. Unfortunately, their lack of a simple tunable structure has inhibited their evolution and applicability in new avenues. Thus, another porous material which has caught much attention is the emerging family of crystalline, 3-dimensional metal-organic frameworks (MOFs). These consist of metal ion clusters that are bound to organic linkers via coordination bonding to form microporous networks, with unique properties that depend on the structure and coordination of the organic linkers and metal ions used. Some of the more attractive features of these materials are their potential application within energy storage, catalysis and gas filtration due to their structural tunability and affinity towards certain molecules. A lot of research has been put into the synthesis of these porous materials and over 6000 MOFs have been published each year since 2016. Although, according to [2] there are still significant challenges in manipulating their morphologies, dimensions and processability as they often are insoluble and brittle, rendering them very difficult to handle during post-process and manufacturing. It has been shown that a substrate as template for the growth of a MOF could be used in order to obtain chemically integrated hybrids with MOF crystals grown upon their modified surface [3]. For example, there have been reports of configuring MOF crystals within matrices of metal oxides or polymeric substrates in order to process them as thin film membranes and porous beads. Albeit, these hybridized MOFs still lack the flexibility and shapeability necessary to effectively limit their manufacturing shortcomings [4]. Thus, there has been a rising interest in functionalizing biopolymers which are environmentally friendly, ductile and shapeable to act as templates upon which MOF crystals would grow upon and potentially use them within the industry, e.g., as filter membranes for gas separation.

The project at hand will focus on nanoengineering of metal-organic framework materials by surface modifying *Cladophora* cellulose to develop freestanding hybrid nanocomposite papers of

MOFs attached to the surface of cellulose. The results given by the study to be conducted may open new avenues on how nanomaterials may be implemented in the industry.

1.2 Project aim

The main goal of this thesis project is to utilize a state-of-the-art interfacial synthesis approach to try and synthesize two sub-types of MOFs; zeolitic imidazolate framework-67 (ZIF-67) and zeolitic imidazolate framework-8 (ZIF-8) on the surface of cellulose nanofibers (CNF) to develop nanocomposites of CNF@ZIF-67 and CNF@ZIF-8. The ZIFs have been proven to showcase increased surface area versus comparable zeolites and showcase chemical- and thermal robustness. The substrate used for the integrated nanocomposites will be surface modified nanofibrous cellulose stemming from a specific type of green algae, *Cladophora*. The surface modification will be a combined result from TEMPO-mediated oxidation and subsequent ion-exchange. These ion-exchanged surfaces of the cellulose nanofibrils will act as anchoring sites, on which ZIF-67/ZIF-8 crystals may nucleate and grow upon in-situ. A series of experiments will be conducted to observe if there is a correlation between the morphology of the ZIFs crystals upon the CNFs and metal salt concentration. Desirably, a core-shell structure between the nanocellulose fibers and ZIF crystals will be devised. Furthermore, a proof-of-concept to use one of these nanocomposites as selective CO_2 filter membranes is demonstrated for potential applicative use.

2. Theory

2.1 Cladophora Cellulose

Cladophora algae are a type of green algae which bloom and grow prominently in coastal regions, their growth being mainly triggered by industrial pollutants in water [5]. The aquatic life is affected the most when these algae age and die, forming dense mats on the surface of the water and drift away as a consequence of wind action. As time passes, the filamentous algae eventually drop down to the seabed where they decompose. The decomposition process is initiated by nearby bacteria and the dead algae are perceived to be very nutritious to them, allowing for the bacteria to thrive. The combination of over-nutrition and loss of oxygen supply, as the decomposition process consumes oxygen, results in a weakening of functioning marine ecosystems in the nearby region. According to [5], the physical removal of such algal mats on the seabed was proven to be beneficial to the marine life and restored balance to any present ecosystem. Subsequently, there was a rising interest to explore whether or not the removed *Cladophora* algae could potentially be used as a resource, especially their cellulose.

Cellulose is a renewable and abundantly available biopolymer that is found as a major constituent in plant fibers, bacteria's and in different families of algae, such as the green algae *Cladophora*. It is one of the most occurring biopolymers on Earth and was first extracted from tissues of plants by Anselme Payen in 1838 [6]. The biopolymer is composed of polysaccharides with a repeating molecular unit defined as *D-anhydrous glucopyranose ring unit* (AGU). One of the monosaccharides, which composes the polysaccharide as a whole, is bound to the other monosaccharide via a covalent β(1→4) glycosidic oxygen linkage which the polymer chain is able to rotate, bend and twist around. There is a total of three alcohol groups per monosaccharide. The primary alcohol group is located on C6, while the other two secondary alcohol groups are on C2 and C3, respectively, as can be seen in Figure 1. The oxygen atoms which are present on the cellulose chain will, together with the hydroxyl groups, generate strong hydrogen bonds and give rise to hydrophilic properties in aqueous solutions. The hydrogen bonds may occur between adjacent polymer chains too, which yield cellulose microfibrils and is the main cause as to why this biomaterial is rather insoluble in most solvents [7].

Cellulose from *Cladophora* has a native hierarchical structure due to the reoccurring hydrogen bonds between adjacent chains. The polymer chains are continuously stacked around each other in crystalline and amorphous domains [8]. The accumulation of these polymer chain stacks contributes to a hierarchical, fibrous structure that is defined by interfiber voids, giving rise to a mesoporous structure with a high surface area of ~100 m^2/g. This is a larger value than cellulose from different origin. These structures are then assembled into larger microfibrils which constitutes the cellulose fibers in plants and algae. Measurements revealed that the degree of crystallinity in *Cladophora* cellulose could be as much as 95%, which is higher compared to cellulose from a variety of plants and bacteria.

Disintegrating cellulose fibers to obtain the building block fibrils is called fibrillation and has found industrial interest as it opened up for an effective way of surface modifying individual cellulose fibers and functionalizing them [9]. Fibrillation of *Cladophora* cellulose may yield very long, rigid nanofibrils with high aspect ratios that may be dispersed in aqueous solutions, which provide an excellent solution-based approach to organize and prepare the nanocellulose for surface modification. Obtaining nanocellulose from *Cladophora* often yields fibers with diameters ranging from ~25-30nm. The high degree of crystallinity makes the cellulose an excellent candidate for chemical modification and ultrasonication defibrillation without completely destroying its structure.

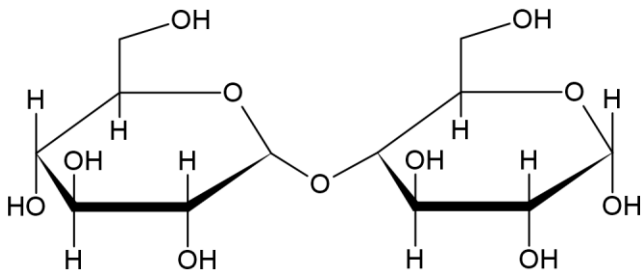

Figure 1. AGU of cellulose**.**

2.2 TEMPO/NaBr/NaClO Oxidation (TEMPO-CNFs)

As mentioned in 2.1, *Cladophora* nanocellulose exhibits excellent properties to be used as a template for growth of nanomaterials on it. One interesting property that all type of investigated cellulose have in common is the abundancy of hydroxyl groups that may act as chemical sites for surface modification of the cellulose in question [10]. In the past decade, high-energy ultrasonication has been used to obtain fibrillar structures of the cellulose denoted as micro- and nanocellulose, although this alone has never yielded a very high degree of individualized fibrils. Instead, the fibers were found to be bundled together non-homogenously to some degree, suggesting remaining presence of hydrogen bonds [11]. Another route consists of chemical modification of the cellulose surface to facilitate the separation of bundled fibrils at their amorphous regions by treating cellulose in sulfuric acid, although the fibril length and yield is significantly reduced by 30-50%. This treatment yields crystalline nanocellulose (CNC). In order to increase the yield of nanofibrils and attempt to retain their lengths, another chemical modification has been proposed. This method conceptualizes the selective oxidation of the primary alcohol on the C6 position to a carboxylate group. This method allows for cellulose microfibrils to be effectively liberated into elementary nanofibrils, by using TEMPO (*2,2,6,6-tetramethylpiperidin-1-oxyl* radical) and was first utilized by De Nooy et al. [12]. The aforementioned method was diligently used in this master's thesis for surface modification of the *Cladophora* cellulose to obtain cellulose nanofibers (CNFs) in combination with ultrasonication.

TEMPO, a nitroxyl radical, is in itself a rather stable molecule due to the presence of bulky side chains. It may be converted into a *nitrosonium cation* ($TEMPO^+$) in the presence of stoichiometric amounts of a primary oxidant, *sodium hypochlorite* (NaClO), and *sodium bromide* (NaBr) as co-catalyst in an aqueous solution. The $TEMPO^+$ is the true oxidant of the -OH group and oxidation yields an aldehyde intermediate that is further converted into a carboxylate group. Following oxidation of the alcohol, the $TEMPO^+$ is reduced to a *hydroxylamine* which may be re-oxidized in the presence of NaBrO, being NaBr that has been oxidized by NaClO, to regenerate the oxidation cycle. A reaction mechanism suggesting how C6 hydroxyl groups are converted into carboxylates is presented in Figure 2.

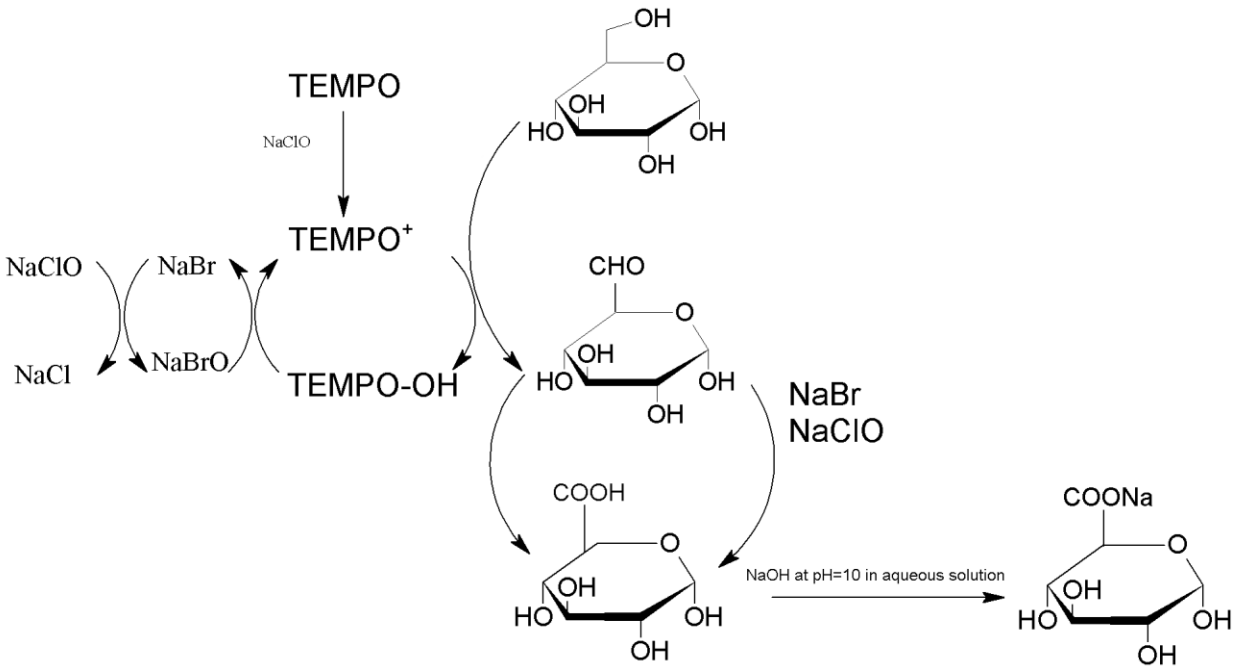

Figure 2. TEMPO-mediated oxidation of -OH at C6**.**

The end-result of the oxidation process is heavily pH dependent as the carboxylate moiety may either be in protonated form at lower pH or in deprotonated form in alkaline conditions [13]. In general, acidic carboxyls are formed during the reaction and it was shown that the most effective oxidation occurred within a pH window of 10-11. Thus, it is of importance to maintain a stable pH by adding a certain amount of *sodium hydroxide* (NaOH) that may be consumed during the reaction until the pH remains at a static value of ~10. For aqueous solutions of cellulose being oxidized under alkaline conditions (~pH 10), the C6 -OH groups on the surface of the cellulose is converted into *sodium carboxylate groups* due to presence of Na^+ which the negatively charged carboxylate groups may bind with. Some chemical bonds may still be present between neighboring fibrils as the degree of oxidation may vary depending on the duration of the reaction. These may be broken via ultrasonication, yielding fine individual *TEMPO-oxidized nanocellulose fibrils* (TEMPO-CNFs) dispersed in the aqueous solution.

2.3 Ion-exchange of the TEMPO-CNFs

Native cellulose, from any of the aforementioned sources, are initially free from viable functional groups which may promote growth of material upon the surface. Thus, anchoring capabilities with potential metal ions for in-situ growth of ZIF nanoparticles are severely inhibited. Following the TEMPO-mediated oxidation, the formed carboxylate groups will be attached to the sodium ion via ionic bonding as can be seen in Figure 3. This sodium ion will be feasible for an ion-exchange with other metal ions. By allowing the TEMPO-CNFs to soak in metal salt solutions over a period of time, ion-exchange may be initiated [14].

This opens up venues for the TEMPO-CNFs to act as a substrate for potential growth of material, such as in this case; growth ZIFs. The sodium ion can be ion-exchanged with a metal ion which the particular ZIF is composed of and act as an anchor site for the attachment of organic ligands. This subsequently leads to the growth of the ZIFs following addition of more metal salt and organic linkers into the ion-exchanged TEMPO-CNFs solution [15].

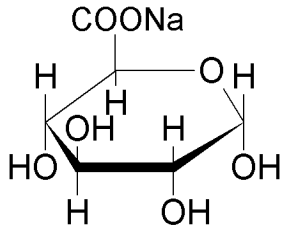

Figure 3. Introduction of a sodium carboxylate group on C6 thanks to TEMPO-mediated oxidation. The sodium ion may be viable for ion-exchange**.**

2.4 Polyvinylpyrrolidone (PVP)

Polyvinylpyrrolidone (PVP) is an amphiphilic and non-toxic polymer that may be used in a variety of ways during nanoparticle synthesis, such as an encapsulating agent of various metal oxides or capping agent to promote growth of nanoparticles to specific shapes by capping specific surfaces of the particle nuclei in question [16]. The repeating unit is composed of two constituents; a hydrophilic pyrrolidone moiety that is polar due to the amide group and a hydrophobic alkyl group which is non-polar. Thus, its amphiphilic nature stems from these two respective components. It has been shown that it can act as an excellent stabilizer, making sure that nanoparticles in a solvent do not aggregate. In this work it was used as a crystallization- and interfacial stabilizing agent between the ZIFs and the TEMPO-CNFs as per methods utilized by Zhou et al [17].

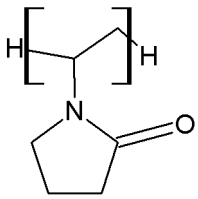

Figure 4. Repeating unit of PVP where the polar amide group and non-polar alkyl groups are depicted**.**

2.5 Metal-organic frameworks (MOFs)

Metal-organic frameworks (MOFs) are crystalline materials with extensive surface areas, which stems from their microporous nature. They consist of metal cations, linked to an organic linker via coordination bonding [18]. This, subsequently, leads to the formation of a network that extends with repeating coordination clusters in a periodic manner through space, forming a long-range ordered framework. Common metals used are the ones from the transition series such as Fe^{3+}, Co^{2+} and Cr^{2+}. Alkali- and alkaline earth metal ions have also been reported for the formation of various MOFs with different properties [19]. During most synthesis routes, the metal ions are commonly present as precursors such as nitrates, acetate, chlorides or oxides. The organic linkers, by which the metal ions or clusters are attached to coordinatively, may contain functional groups such as carboxylates, imidazole's, sulfonates, phosphates, amines or nitriles. Therefore, the choice of metal ion and organic linker dictates not only the structure, but the MOFs intrinsic properties as well.

The reason as to why MOFs have garnered so much attention over the past few years is due to the fact that their surface areas, according to [18], most often exceeds the value for other comparative porous compounds such as activated carbons, zeolites and mesoporous silica by large values. One of the most prominent merits of MOFs is their topological diversity. By exploiting the philosophy which conceptualizes reticular chemistry, the science of combining molecular building blocks, scientists have been able to produce various tailored MOFs using a plethora of different metal ion-organic linker combinations [20].

There are different routes to synthesize MOFs. Common methods are solvothermal, hydrothermal and non-solvothermal methods, such as ball-milling and mechanical grinding. A few other unconventional methods have been reported such as microwave-assisted synthesis, layer-by-layer synthesis and sonochemical synthesis. Room temperature synthesis have also been explored due to its potential for less energy consumption and ease of performance. [21, 22].

Many factors affect the synthesis of MOFs, thus, trying to manipulate parameters to enhance or stabilize certain properties has been a challenge for many [24]. The major synthesis parameters that has been subjects of interest are the type of solvent used, pH, metal-ligand ratio and temperature. The solvent in question has been deduced to play a part on the morphology of the crystal/formation of the MOF. Most often, choice of a specific solvent is based on the solubility of the starting materials and proteolysis property of the organic linker.

2.6 Zeolitic Imidazole Frameworks (ZIFs)

As stated in previous sections, microporous aluminosilicate-based materials known as zeolites have had a big impact in the industry mostly due to their surface areas resulting in high catalytic abilities, sensing and gas storage [25]. Even though their use has been established commercially, modifying their structures to enhance their properties for, e.g. CO_2 absorption, has been largely unrealized due to difficulties fine-tuning their structures to promote CO_2 affinity. Instead, during recent years, Yaghi et al [26] discovered a plethora of framework compounds which had superior properties compared to other porous materials with industrial potential as, e.g., CO_2 capture.

Zeolitic imidazolate frameworks, also known as ZIFs, have recently emerged as a sub-class of the MOFs. They are porous, crystalline and share a similarity in structure with zeolites. ZIFs consist of metal ions which coordinate tetrahedrally, such as Zn^{2+}, Co^{2+}, Fe^{2+}, with imidazole-type organic linkers [25]. The angle at which the organic linker bridges with the metal ion is ~145°, which is similar to the silicon-oxygen-silicon angle found in zeolites, resulting in their isomorphic porous structure. This has led to the synthesis of different ZIFs with remarkable properties, exhibiting permanent porosity, exceptional thermal- and chemical stabilities, making them excellent potential candidates for industrial applications. As they share traits stemming from both zeolites and MOFs, ZIFs combine the structural tunability of a MOF with the chemical- and thermal stability of a zeolite. Alas, they do retain weaknesses similar to other MOFs, such as low post-processability and high brittleness. The pristine product obtained is most often a powder, which precipitates out of solution during solvent-based synthesis.

There have been a handful of ZIFs which have been synthesized since their discovery. During this thesis project ZIF-67 and ZIF-8 will be synthesized in room temperature and used as the components, respectively, to be grown in-situ upon the TEMPO-CNFs. These ZIFs will be synthesized in methanol (MeOH) and composed of tetrahedrally coordinated *2-methylimidazole* (2-MIM) linkers bridged with a Co^{2+}-ion for ZIF-67 and Zn^{2+}-ion for ZIF-8. A proposed reaction scheme has been deduced, which can be seen in Figure 5, and the reaction steps involved may be categorized as:

- Linker coordination of Zn^{2+}/Co^{2+} centers.
- Deprotonation of the 2-MIM linker.
- Oligomerization of Co^{2+}-(deprotonated 2-MIM) complexes leading to complete structure.

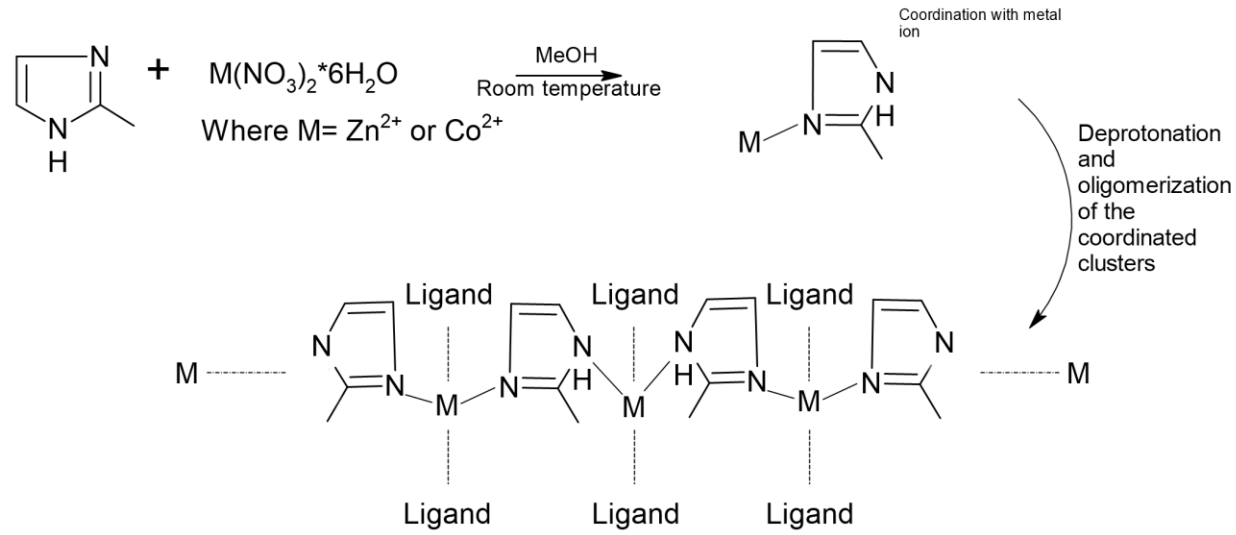

Figure 5. Proposed general reaction mechanism for the formation of ZIF-67 and ZIF-8 in MeOH, the former obtained by using cobalt ions while the latter requires zinc ions**.**

The synthesis of ZIF nanoparticles have usually been performed in an organic solvent, thus the choice of using MeOH in this thesis work. Synthesizing in a mixture of an organic solvent with deionized water has also been done [27, 28]. Although, the latter and even pure deionized water was proven to yield very different morphologies for ZIF-67 with e.g. lower BET surface areas and dense structures compared to its counterpart synthesized in MeOH. One of the causes was the apparent sensitivity to moisture these compounds retain during synthesis, especially ZIF-67. Pure-phase ZIF-8 has been obtained with certain crystallinity but lower yield during room temperature aqueous synthesis.

Recent studies involving the deduction of the degradation mechanism, in order to understand their sensitivity, when MOFs and ZIFs are exposed to water revealed that hydrolysis or ligand displacement are the culprits for structure failure [29]. The ligand displacement reaction follows as:

$$M^{n+} - L^{n-} + H_2O \rightarrow M^{n+} - (OH_2) \dots L^{n-} \qquad (1)$$

As can be seen from the reaction formula, a water molecule is inserted between the metal-ligand bond, leading to a hydrated cation and release of a ligand, collapsing the framework. During hydrolysis, the metal-ligand bond is fully broken while a water molecule dissociates, forming a hydroxylated cation and a protonated ligand that is released. The hydrolysis reaction scheme follows as:

$$M^{n+} - L^{n-} + H_2O \rightarrow M^{n+} - (OH)^- + HL^{(n-1)-} \qquad (2)$$

In order for proper formation of ZIF nanocrystals and control over particle size, one of the most important parameters related to synthesis of ZIFs has been found to be the molar ratio between metal ions and organic linkers [30]. An increased amount of organic linker results in a higher number of deprotonated ligands which the metal ion may coordinate with accordingly. Additionally, by adding a heftier number of organic linkers, the excess ligands may cover nucleated crystal seeds and allow inhibition of prolonged crystal growth. Consequently, this leads to rapid nucleation, favoring smaller ZIF nanocrystals over larger ones. However, the amount of organic linker needed to form nanocrystals of ZIF-8 and ZIF-67 have been reported to be at least ~20-100 times more than the metal ions, especially in water. Hence, the more deprotonated ligands obtained, the more feasible the ZIF- nanoparticle formation will be.

By addition of a deprotonating agent with basic character, the 2-MIM linker used to synthesize ZIF-8 and ZIF-67 have been shown to rapidly deprotonate and allow for a higher nucleation rate to take place, simultaneously inhibiting prolonged crystal growth. Hence, this method favors the nucleation and formation of small crystals, at lower required amounts of 2-MIM for formation of ZIF-8/ZIF-67 from $Zn(NO_3)_2 \bullet 6H_2O$/ $Co(NO_3)_2 \bullet 6H_2O$ and 2-MIM in the presence of triethylamine (TEA). This suggests that a minimum amount of 2-MIM may be used for successful formation of ZIFs when TEA is included during synthesis.

2.7 CNF@MOFs

Structuring and assembling of MOFs on templates in order to facilitate their application uses in an industrial scale has been a topic of high interest. Such modifications may result in composites fit for air filtration, gas storage and catalytical endeavors. Research has been put into using different templates and substrates in order to facilitate both the assembly during synthesis and their manufacture processing. The results were hybridization of MOFs with either polymers or metal oxide matrices in order to assemble them as a variety of structures ranging from thin films, porous beads, dense pellets and hierarchical monoliths [31]. Although, most of these polymers used are synthetic and a product of derivatives from the petrochemical industry and possess risks of health- and environmental degradation if scaled-up. Beside their toxic nature, one of the major difficulties regarding polymer-MOF composites have been the absence of desirable rigidity and flexibility. Another difficulty has been the fact that most of these hybrid nanocomposites have been developed with complicated experimental procedures, which effectively hampers their rate of production on an industrial scale. For example, there have been attempts to synthesize MOF particles upon polyacetonitrile nanofibers using microwave radiation, albeit the nanofibers melted due to the irradiation and the composites structure was heavily affected [32]. These difficulties have caused significant setbacks of advancing such hybrid materials from lab scale to industrial scale.

Therefore, there has been a wide interest in implementing biopolymers as a means to be used as templates for incorporation of MOFs, allowing for enhanced post-processability of the MOFs and simultaneously decreasing the composites inherent environmental toxicity. These originate from natural resources with intrinsic ductile properties. They come in abundant amounts and add flexibility alongside shapeability to the nanocomposite and allow MOFs to be applied in various applicable ways. Examples of biopolymers that have been used to produce composites of MOFs are surface modified chitin and cyclodextrin as effective encapsulating-, gas sequestering- and drug-delivery agents [31].

Recently, cellulose has been proven to be able to be used as a substrate for facile incorporation of MOF particles within the cellulose fiber matrix. By combining properties stemming from both the cellulose and the MOF particles, the composites could be used for effective filtration of organic dyes, polluted solutions containing heavy metals and gas separation [15, 33, 34]. Albeit, the MOF particles are only randomly dispersed within the cellulose matrix and are primarily held in place merely due to the physical entanglement arising from the fibrous network and weak van der Waals forces [15]. Thus, the shapeability and processability of these composites would be further enhanced if controlled growth of the actual MOF particles could be induced upon the individual nanocellulose fibers via chemical bonds which would allow for the fabrication of freestanding membranes.

Zhou et al [17] succeeded in producing sophisticated nanocomposites of a plethora of MOFs with *Cladophora* cellulose as the substrate of choice, defined as CNF@MOFs. The nanocomposites were synthesized by assembling MOFs onto TEMPO-oxidized and ion-exchanged nanocellulose fibers (TEMPO-CNFs). By using a process of filtration, drying and mold pressing, freestanding

CNF@MOF nanopapers were also achieved. The MOF crystals had a layered morphology, wrapping the individual TEMPO-CNFs.

2.8 Gas sorption for porosity and surface area analysis (N_2 gas sorption)

Gas sorption may be used as a means to characterize the porosity, pore size distribution and surface area of porous materials [35]. There are two different types of surface adsorption; physisorption and chemisorption. The former occurs when molecules attach to the surface via London-dispersion forces. Chemisorption occurs when adsorbents bind themselves by chemical bonding with the atoms present on the open surface and is therefore much stronger than physisorption. Lowering the temperature facilitates the adsorbents to attach to the surface through London forces, instead of forming ionic and/or covalent bonds which are difficult to break. Commonly, nitrogen gas is used at a temperature of 77 K as this allows the nitrogen molecules to attach to the surface of the material via physisorption in a reversible fashion for the sake of characterization.

According to IUPAC there is a set of proposed definitions for different types of adsorption isotherms, relating the number of adsorbed molecules and the relative pressure to a given porosity type which can be seen in Figure 6. While performing adsorption-desorption measurements, the obtained isotherm may be characterized accordingly. The Brunauer-Emmet-Teller, BET, surface area and pore distribution of a sample may also be calculated using this type of measurement.

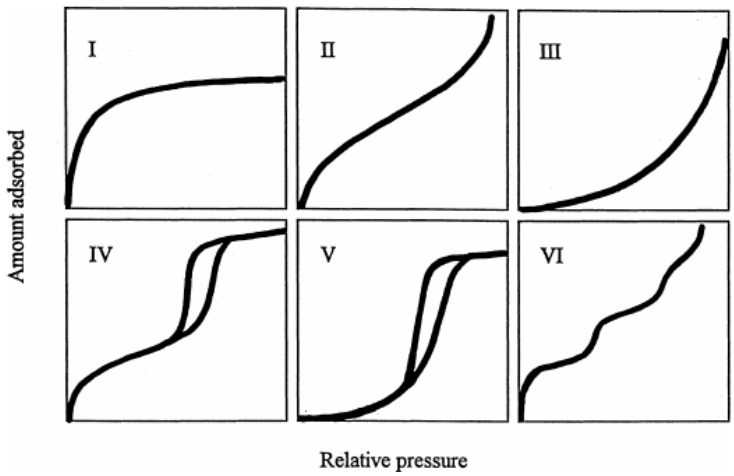

Figure 6. IUPAC classification on adsorption isotherms [35]. Type I refers to a microporous adsorbent with pore sizes smaller than 2 nm, type II, III and VI non-porous/microporous materials with pore sizes of 2-50 nm while type IV and V is characteristic for mesoporous materials which have a pore size greater than 50 nm**.**

3. Experimental

3.1 Materials

Cladophora cellulose powder provided by Dr. Chao Xu. *Sodium bromide* (NaBr), *2, 2, 6, 6-tetramethylpiperidine-1-oxyl* (TEMPO), *sodium hypochlorite* solution (NaClO, 10%), *2-methylimidazole* 97% was purchased from Alfa Aesar, *polyvinylpyrrolidone* (PVP, Mw = 3.6 × 10^5 g/mol), *triethylamine* (≥ 99%), *sodium hydroxide*, *hydrochloric acid*, *cobalt(II) nitrate hexahydrate, Zinc(II) nitrate hexahydrate* 98+% were purchased from Sigma-Aldrich without further purification. *Methanol* of isocratic grade was purchased from VWR Chemicals.

3.2 TEMPO-mediated oxidation the cellulose

Initial experiments conducted for the synthesis of the composites were mostly considered as failures, many of which stemmed from several of the TEMPO-oxidized nanocellulose batches that were made in the beginning due to difficulties calibrating the concentration of the TEMPO-CNFs solution. Thus, the first few batches of TEMPO-CNFs were considered a part of a trial and error approach until viable batches were produced. Below is an in-depth description of methods utilized for the final TEMPO-CNFs batch which was used for successful synthesis of CNF@ZIFs nanocomposites.

In order to remove any present impurities before the oxidation, 1 g of the Cladophora cellulose powder was washed in a 200 mL NaOH aqueous solution (0,5 mol/L) for 24 hours prior to the TEMPO-mediated oxidation. The solution was stirred at 450 rpm using a magnetic stirrer. As the NaOH was readily available in pellet-form, to prepare a 200 mL 0,5 mol/L solution, 4 g of NaOH pellets were dissolved in deionized water.

The 200 mL solution was divided into 4, 50 mL tubes and centrifuged repeatedly at 3,800 rpm for 15 minutes with deionized water in order to neutralize the cellulose and prepare it for the TEMPO-oxidation. After each cycle, a litmus paper test was conducted in each tube to assure that the pH was as close to 7 as possible. The sedimented cellulose flocculates were collected from each tube and put into a sonication beaker along with 100 mL of deionized water. Ultrasonication with a probe was conducted for 10 minutes with a pulse length of 10 seconds and a pause of 10 seconds with a power amplitude of 60 % under running, cool water. After sonication, the thick cellulose hydrogel was transferred into another beaker for TEMPO oxidation.

By adding a 10 mL aqueous solution of 16 mg TEMPO and 100 mg NaBr to the cellulose, the TEMPO-mediated oxidation was initiated with the addition of 3,1 mL NaClO. The solution was continuously stirred at 650 rpm. Immediately, the pH rose to 12 after adding the NaClO due to its alkaline nature. After a while, the pH started slowly decreasing, hence confirming the initiation of the oxidation reaction. The oxidation occurred for 6 hours. Solutions of NaOH and HCl with the concentrations 0,5 mol/L were prepared and added to the solution every 30 minutes to ensure that

the pH of the solution was at ~10 during the whole oxidation process, as it tended to continuously drop until no further NaOH was able to be consumed. In order to observe the pH, a pH meter was used.

The TEMPO-CNFs was then washed with deionized water by vacuum filtration with a PVDF membrane with a pore size of 0,1 µm several times in order to try and remove any unreacted reagents, inorganic salt etc. The obtained hydrogel of oxidized cellulose was then collected and put into the sonication beaker to be sonified once again for 10 minutes with 10 second pulses and 10 second pauses with a power amplitude of 60% in 100 mL deionized water. The concentration of the TEMPO-CNFs suspension was then calibrated by allowing 1 mL of the solution dry in a furnace at 70^{o} C for several hours until a dry film was obtained. The dry cellulose film was weighted and had a mass of 7,33 mg. Thus, the suspension had an estimated concentration of 7,33 mg/mL and was put into a fridge for further experiments.

3.3 Synthesis of CNF@ZIF-67 and CNF@ZIF-8

As outlined in section 2.3, there are many ways to synthesize MOFs and ZIFs. The synthesis of pristine ZIF-67 and ZIF-8 has been performed and reported in ambient conditions with MeOH as solvent and TEA as a deprotonating agent [30, 36].

3.3.1 Solvent-exchange of the TEMPO-oxidized CNFs

5 mL (7,33 mg/mL) of the TEMPO-CNFs solution was solvent-exchanged by centrifugation 3 times with MeOH at 11,000 rpm for 30 minutes. Between each pass, the cellulose was dispersed in MeOH and shaken 20 minutes in order to achieve as homogenous of a dispersion as possible. The solvent exchanged TEMPO-CNFs was then redispersed in 10 mL of MeOH for ion-exchange. If any flocculates were seen in-between the centrifugation passes even after extensively shaking the TEMPO-CNFs/MeOH solution, sonication was commenced for 15 minutes in order to further homogenize the suspension.

3.3.2 Ion-exchange

The ion-exchange was commenced by mixing a select, excess, amount of $Co(NO_3)_2 \bullet 6H_2O$ in 2 mL of MeOH until dissolved. The slight pink solution was put into the 10 mL solvent-exchanged TEMPO-CNFs solution and stirred at 300 rpm for 1 hour. Later, the solution with the ion-exchanged CNFs was washed several times with MeOH by centrifugation at 11,000 rpm for 30 minutes. The washed and ion-exchanged TEMPO-CNFs was redispersed in 10 mL MeOH. The same procedure was commenced when ion-exchanging for growth of ZIF-8. The only difference being the metal salt used; $Zn(NO_3)_2 \bullet 6H_2O$ for ZIF-8. The reason why an excess amount of metal salt was used was to ensure saturation of the suspension with metal ions and make sure that as

many sodium carboxylate groups were ion-exchanged before washing. For the one-step process, the washing step described above was skipped.

3.3.3 CNF@ZIFs: Synthesis and controlling morphology of ZIF-67 and ZIF-8 crystals upon CNFs

A set of experiments were conducted in order to determine whether the morphology of the grown ZIF-67 and ZIF-8 crystals upon the TEMPO-CNFs could be controlled or not, in relation to the amount of metal salt used. As stated in previous sections, the synthesis of MOFs in general depend on many factors and are complex. Thus, in order to enhance the probability of being able to determine whether or not the amount of metal salt affected the morphology of the ZIF-67/ZIF-8 on the TEMPO-CNFs, other parameters remained as static as possible during synthesis. These included the amount of PVP, molar ratio between TEA, 2-MIM and $Co(NO_3)_2 \bullet 6H_2O$/$Zn(NO_3)_2 \bullet 6H_2O$, concentration of TEMPO-CNFs and temperature. The final molar ratio between metal salt and organic linker was set to 1:5 while for organic linker and TEA was set to 1:1.

After washing the ion-exchanged TEMPO-CNFs, the calculated amount of metal salt and PVP were dissolved in 2 mL of MeOH in a 15 mL test tube (*Component A*). In another 15 mL test tube, 2 mL of 2-MIM and TEA (*Component B*) were mixed vigorously. Component A was put into the ion-exchanged TEMPO-CNFs solution and stirred for approximately 20 minutes, allowing the PVP to activate the surface of the nanocellulose fibrils. Subsequently, Component B was poured into the solution and stirred overnight. The amount of each reagents used for the synthesis of successful CNF@ZIF-67 and CNF@ZIF-8 samples are listed in Tables 1 and 2. Finally, the products were washed with MeOH 3 times in order to remove as much of any unreacted reagent as possible.

Table 1. Reagents used for synthesis of CNF@ZIF-67 using two-step process**.**

$Co(NO_3)_2 \bullet 6H_2O$ (mg)	**TEA (µL)**	**2-MIM (mg)**	**PVP (mg)**	**CNFs (mg)**	**Definition**
15	36	21.1	10	36,65	CNF@ZIF-67:A2
20	49	28.3	10.05	36,65	CNF@ZIF-67:B2
25	60	35.2	10	36,65	CNF@ZIF-67:C2

Table 2. Reagents used for synthesis of CNF@ZIF-8 using two-step process**.**

$Zn(NO_3)_2 \bullet 6H_2O$ (mg)	TEA (µL)	2-MIM (mg)	PVP (mg)	CNFs (mg)	Definition
15	35	20.6	10	36,65	CNF@ZIF-8:A2
20	46,8	27,5	10	36,65	CNF@ZIF-8:B2
25	58,5	34,45	10	36,65	CNF@ZIF-8:C2

For each of the above-mentioned experiments, a dark purple solution was obtained for CNF@ZIF-67, while a milky white solution was obtained for CNF@ZIF-8. These colors are characteristic of ZIF-67/ZIF-8 formation in solution and could be seen in their respective paper formats too, which may be observed in Figure 7 [33]. The freestanding nanopaper of the CNF@ZIFs nanocomposites were obtained by putting respective solution of CNF@ZIF through a vacuum filtration device with a PVDF membrane which had a pore size of 0.1 µm. The filter cake was set to dry for an hour with the vacuum on. Later, the PVDF membrane with the filter cake was removed and another PVDF membrane was put upon it. The sandwiched filter cake was then pressed between two metal plates and put into a furnace at 70^{o} C for 5 hours. The formed nanocomposite paper was then carefully removed by manually peeling it off the filter paper with a pair of tweezers.

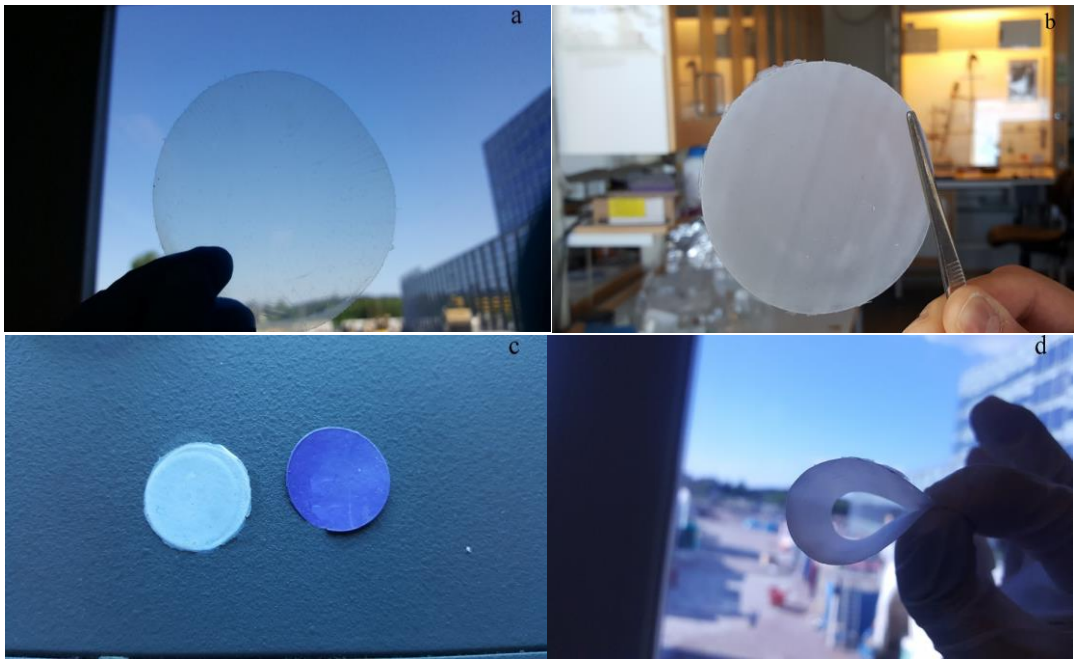

Figure 7. (a) Pure TEMPO-CNFs nanopaper. **(b)** CNF@ZIF-8 scaled up nanopaper. **(c)** CNF@ZIFs "Lab"-scale nanopapers. **(d)** The CNF@ZIF papers are very shapeable and flexible. Notice the characteristic colors of ZIFs on the individual nanopapers**.**

In order to demonstrate the scalability, each type of nanopaper was scaled up once, thus the papers obtained were bigger in comparison to the "lab"-scaled ones produced for structural- and thermal characterizations only. The reason also being that the smaller versions were too small and, e.g. the N_2-sorption requires a certain mass in order to yield measurable results. Unfortunately, the CNF@ZIF-67 nanopaper was too thin to peel off in one whole piece and be showcased.

Also, during this thesis project, experiments for CNF@ZIF-67 were initially conducted in a *two-step process* involving an extra washing step between the ion-exchange and the final synthesis of the nanocomposites, while at a later stage they were conducted in a *one-step process* and then, finally, once again in a two-step process. The two-step process was the official approach.

The one-step process was conducted only to figure out whether or not it was possible to form ZIF-67 crystals in the solvent-exchanged TEMPO-CNFs solution. Formation of ZIF-67 was particularly difficult in the beginning when the two-step process was used. Thus, it was a necessity to follow the one-step process in order to control the formation of ZIF-67 crystals upon the CNFs, before the two-step process could be commenced which washes away most of the excess metal-ions in the ion-exchanged solution. Hence, the reason as to why the formation of ZIF-67 failed was speculated to be that there were far too few metal ions left for favorable formation of ZIF-crystals the first few times the two-step process was used.

By properly recalculating molar ratios between the metal salt and organic linker and the inclusion of TEA, the two-step process could be properly utilized to limit the amount of potentially un-anchored ZIF nanoparticles within the CNF@ZIF-67 solution after the ion-exchange, yielding fewer freestanding nanoparticles that would not be anchored the TEMPO-CNFs. Specifically, this meant that there would be less brittleness to the paper, which would help enhance its flexibility and shapeability due to less amount of excess ZIF particles physically mixed within the TEMPO-CNFs.

When the two-step process was deemed a success for formation of CNF@ZIF-67, CNF@ZIF-8 was immediately synthesized via the two-step process. In regard to experiments conducted with the one-step process, amounts of reagents used for this particular method of synthesis will be listed in Table A1 in the Appendix alongside SEM micrographs that were taken of them in Figure F1. Also, solutions of successful CNF@ZIF-67 and CNF@ZIF-8 vs. failed CNF@ZIF-67 are shown in Figure F2.

3.4 Methods of characterization of CNF@ZIFs

3.4.1 *X-ray diffraction* (XRD)

XRD was used in order to confirm the proper synthesis of crystalline CNF@ZIFs nanocomposites with each component constituting the hybrid nanomaterial and ensure whether or not any

contaminants may be present and have caused the formation of unknown phases. Specifically, CNF@ZIF nanopapers were taped onto a metallic holder to create as flat of a surface as possible and put into the XRD instrument. The analysis was conducted in a *Bruker D8 diffractometer* with Cu-Kα X-ray radiation (λ = 0.154 nm).

3.4.2 *Fourier transform infrared spectroscopy* (FTIR)

FTIR was utilized in order to inspect the chemical properties of the nanocomposites and their constituents. The concept behind the method is obtaining a spectrum with wavelengths within the infrared interval for different materials. Raw material was analyzed and, in relation to it, the spectra for the nanocomposites was studied in order to confirm possible chemical changes. The instrument used to record the spectra was a *Bruker Tensor 27* spectrometer in attenuated total reflectance mode (ATR) between 400-4000 cm^{-1} with a resolution of 4 cm^{-1}.

3.4.3 *Scanning electron microscopy* (SEM)

SEM micrographs were obtained in order to observe the surface of the nanopapers to confirm the presence of ZIFs crystals and inspect their morphology on nano- and microscale. Micrographs were obtained with a *Leo Gemini 1530 FEG SEM* instrument with an acceleration voltage of 3kV.

3.4.4 *Thermogravimetric analysis* (TGA)

This is a method used in order to verify the thermal stability of samples by applying a certain thermal profile. The profile may, in summary, be dynamic or static. The samples are then subjugated to the heat in a controlled chemical environment. It is a versatile method that may be used to, e.g. detect mass changes at certain temperatures. Here, TGA was performed in order to observe the thermal stability of the nanocomposites and determine how the in-situ growth of ZIFs crystals may have affected the TEMPO-CNFs substrate. The experiments were conducted in an inert N_2-atmosphere with a gas flow of 60 mL/min over a dynamic heating range from 25-900^o C with a heating rate of 10^o C/min. The instrument used was a *Mettler Toledo TGA/DSC 3+*.

3.4.5 Nitrogen gas sorption

Nitrogen gas sorption was used in order to characterize properties related to the porosity of the nanocomposites. The obtained isotherms were recorded in an *ASAP 2020 V4.03* instrument with N_2 gas at 77 K. Also, isotherms were obtained for CNF@ZIF-8 at 293K with N_2 and CO_2. Prior to analysis the samples were degassed for 10 hours in 100^o C. The surface areas would be calculated using Brunauer-Emmet-Teller (BET) method in the relative pressure ranges of 0.04-0.15 while the pore size distribution was calculated using density functional theory (DFT).

4. Results and Discussion

4.1 TEMPO-mediated oxidation of *Cladophora* cellulose and subsequent solvent-exchange

One of the more frustrating challenges during this thesis project was to prepare a homogenous dispersion of TEMPO-CNFs in MeOH following solvent-exchange from the aqueous environment in which the oxidation had taken place. Both *Cladophora* cellulose in its natural state and TEMPO-

CNFs retain very good hydrophilicity [14]. The former, due to the abundant amount of -OH groups present on the fibrils while for the latter it is mostly because of the introduction of sodium carboxyl groups that also are hydrophilic in nature. Thus, transferring the TEMPO-CNFs from an aqueous solution, in which they already are well dispersed in, caused difficulty to the solvent-exchange process and their dispersion was quite poor. The consequence was TEMPO-CNFs loss between each MeOH washing cycle after centrifugation, resulting in less amount of TEMPO-CNFs for each sample than the theoretically desired value.

Another plausible explanation is that due to the fact that MeOH and water are polar, separating a solute in a mixture of these is relatively difficult. Originally, the centrifugation was supposed to occur at a lower rpm value of 10,000 for 15 minutes. But the amount of CNFs mass that was lost between each cycle was deemed too high, thus a higher rpm and longer centrifugation time was preordained to at least inhibit the amount of TEMPO-CNFs being lost between each centrifugation pass. This made the fabrication of the nanopapers very difficult and tedious in the beginning, due to higher amount of ZIFs particles compared to CNFs in synthesis solution. This caused brittleness and thinning of the manufactured paper and removing it from the PVDF membrane was difficult, which might have been the unfortunate case for the scale-up of the CNF@ZIF-67 nanopaper. In this case, prolonged centrifugation and sonication was used to minimize CNFs loss between each washing cycle.

4.2 Cross-linking due to ion-exchange of the TEMPO-CNFs solutions as preparation for synthesis of CNF@ZIF-67 and CNF@ZIF-8

In order to promote the ZIF particles growth upon the individual CNFs, instead of being physically mixed within the TEMPO-CNFs matrix, metal ions which the ZIFs are, respectively, composed of had to be introduced onto the surface modified CNFs which was explained in Section 2.3 previously.

To ensure that as many sodium carboxylate groups on the surface of the CNFs were ion-exchanged with the respective metals, an excess amount of the specific metal salt was added to the solution to saturate it. This resulted in the solution turning thick and gel-like almost immediately which could be explained by the reaction phenomenon behind the ion-exchange procedure. Metal ions of divalent nature will react ionically with the carboxylic TEMPO-CNFs and promote the formation of cross-linking between carboxylate groups of neighboring cellulose nanofibrils. This is a phenomenon which has also been observed before during a study conducted by Zhu et al when exposing sodium carboxylated CNFs to other multivalent ions such as Cu^{2+} etc. [15]. Thus, the transition from a light suspension to a thicker MeOH gel indicated ion-exchange behavior of the carboxylated CNFs prior to further analysis, as can be seen in Figure 8.

. 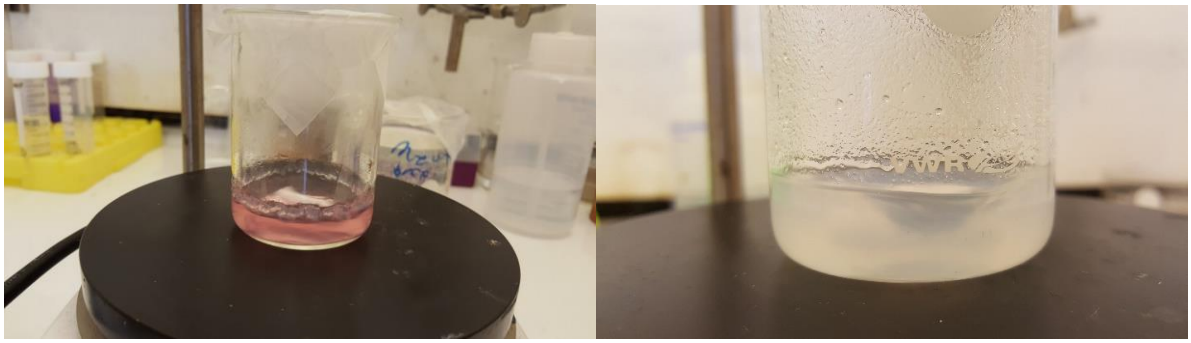

Figure 8. (Left) TEMPO-oxidized CNFs being ion-exchanged with cobalt ions. **(Right)** TEMPO-oxidized CNFs being ion-exchanged with zinc ions. These images represent the gelation of the CNFs suspension due to cross-linking initiated by the ion-exchange procedure. A thickening has occurred and bits of CNFs-$COOCo^{2+}/Zn^{2}+$ MeOH gel can be seen stuck to the walls of respective beaker as the content is stirred**.**

4.3 Analysis of samples

In this section, the synthesis and growth of the ZIFs crystals upon the ion-exchanged and surface modified CNFs were to be analyzed using the series of analytical tools denoted in Section 3.4. Specifically, the presence, attachment and growth of the crystals on the nanocellulose fibers were assessed in order to verify the proper synthesis of the nanocomposites.

4.3.1 Structural- and chemical analysis of CNF@ZIFs nanocomposites

The chemical and structural changes which had occurred during the synthesis of CNF@ZIF nanocomposites were analyzed, in order to verify the synthesis of the nanocomposites and, especially, the incorporation of ZIF crystals on the surface of the TEMPO-CNFs. XRD, FTIR and SEM were diligently used for this portion of the thesis.

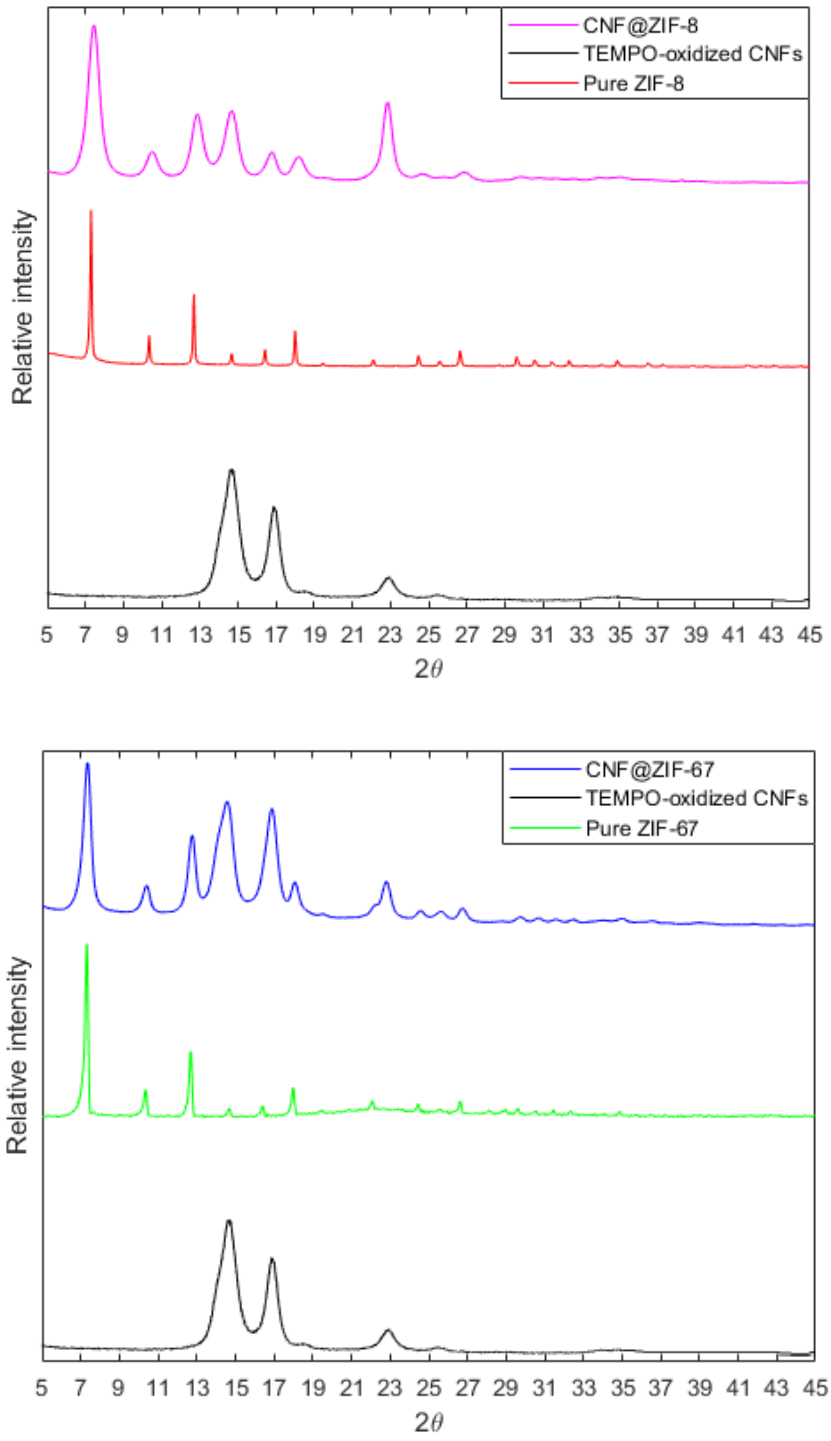

Figure 9. (Top): XRD patterns of TEMPO-oxidized cellulose, pure-phase ZIF-67 and CNF@ZIF-67. **(Bottom):** XRD patterns of TEMPO-oxidized cellulose, pure-phase ZIF-8 and CNF@ZIF-8

The XRD pattern shown in Figure 9 depicts the TEMPO-CNFs versus pure ZIF-67, ZIF-8 and the hybrid nanocomposites. Per literature, the characteristic peaks for ZIF-67 were present and could be observed [37]. The prominent peaks lie at 2θ-values of 7°, 10°, 12°, 14°, 16° and 18° respectively. The peaks were sharp and defined, indicating presence of pure-phase formation of ZIF-67 crystals. The characteristic peaks for the TEMPO-CNFs could also be found at 14,9°, 16,9° and 22,7° which is in accordance with 2θ-values obtained in previous literature [38]. The diffraction patterns for pure ZIF-67 and pure TEMPO-CNFs aligned very well in the XRD pattern for the nanocomposite, suggesting successful incorporation of ZIF-67 crystals on the TEMPO-CNFs without any unknown phases having been formed during synthesis.

The same conclusions could be drawn for the CNF@ZIF-8 nanocomposite. The XRD peaks which may be correlated to pure ZIF-8 had intense reflections at approximately 7°, 10°, 12°, 14°, 16° and 18° which were also in alignment with previous studies conducted on pristine ZIF-8, pointing towards that pure-phase ZIF-8 had been obtained [30]. The peaks from both the TEMPO-oxidized CNFs and pure-phase ZIF-8 is aligned and overlapped well in the CNF@ZIF-8 diffraction pattern. Thus, it could be concluded that successful incorporation of ZIF-8 crystals onto the TEMPO-CNFs had been achieved.

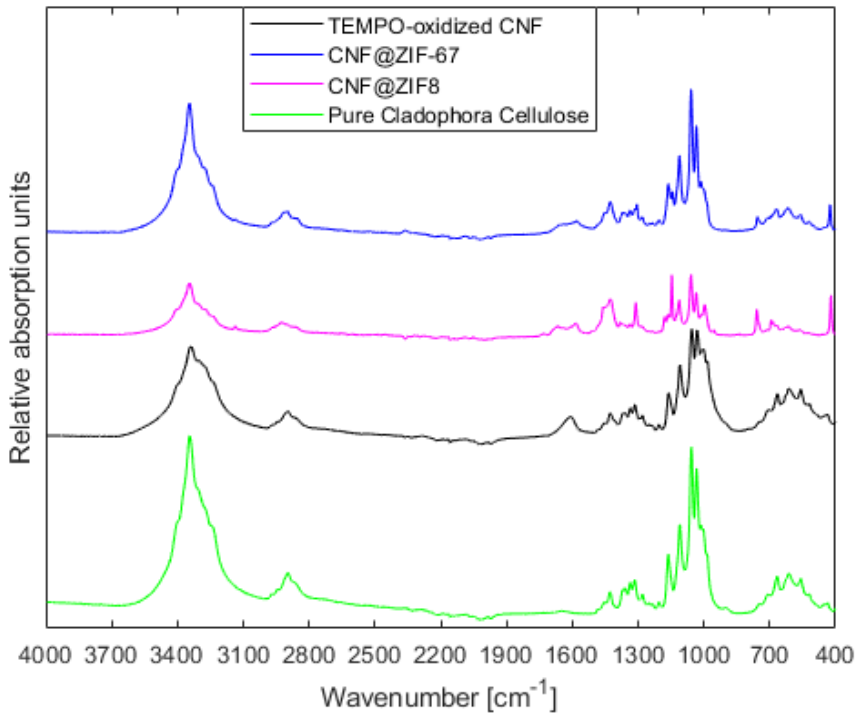

Figure 10. ATR-FTIR of the CNF@ZIFs vs. pure Cladophora cellulose powder and TEMPO-oxidized CNFs. Notice the introduction of the peak at ~1612 cm^{-1} representing the stretching of the carboxylate group the surface of the TEMPO-oxidized Cladophora cellulose. Then, after a change in chemical environment of the carboxylate group on the CNFs due to ion-exchange, it shifts and decreases for both composites.

Characteristic absorption bands in the ATR-FTIR spectra for the *Cladophora* cellulose could be readily observed at 3344 cm^{-1} , 2897 cm^{-1}, 1315 cm^{-1}, 1161 cm^{-1}, 1059 cm^{-1} and 898 cm^{-1}, depicting the -OH stretching, C-H stretching, H-C-H wagging vibration and C-O-C asymmetric bridge stretching of the β-glycosidic linkage between anhydroglucose units, C-O-C pyranose ring skeletal vibrations and deformation of the β-glycosidic linkage in Figure 10 [39]. Comparing these absorption bands with those observed for the TEMPO-oxidized CNFs, a difference in the absorption spectra was found at ~1612 cm^{-1}. The existence of this absorption band corresponded to the stretching vibration of the carboxylate group which had been introduced after oxidation of the C6 hydroxyl groups on the *Cladophora* cellulose. This finding confirmed that the TEMPO-mediated oxidation had been a success. Furthermore, looking over at the spectra depicting the CNF@ZIFs nanocomposites, new absorption bands had appeared signifying several chemical changes. One of the major changes was correlated to the carboxylate stretching vibration absorption peak at ~1612 cm^{-1} that was discussed earlier, which had shifted and dampened for both CNF@ZIF-8 and CNF@ZIF-67. As mentioned in Section 2.3, the concept behind the interfacial synthesis of ZIFs and MOFs on CNFs overall is that there needs to be specific sites at the surface of the cellulose on which the MOF/ZIF can attach to and grow upon. Thus, either Co^{2+} or Zn^{2+} may ion-exchange with the sodium ion and bond ionically to the carboxylates. The explanation as to how metal ions bonded with the carboxylates after ion-exchange was through the free, delocalized electron of the carboxylate group. This change in chemical environment, from being bound with Na^{+}- to either Co^{2+} or Zn^{2+} ions, affected the stretching vibrational mode of the carboxylate group and is seen as a shift of the peak, consequently indicating ion-exchange [40]. Additionally, for TEMPO-CNFs, CNF@ZIF-67 and CNF@ZIF-8, the -OH peak at 3344 cm^{-1} had undergone a slight broadening and shifted, compared to pure *TEMPO-CNFs* which is consistent with the study conducted by Zhu et al as they prepared MOFs aerogels templated by ion-exchanged TEMPO-CNFs.

Also, characteristic peaks for respective ZIFs could be located in each absorption spectra of the nanocomposites. The absorption bands at 3135 cm^{-1},1448 cm^{-1}, 1580 cm^{-1}, 1142 cm^{-1}, 756 cm^{-1} and 426 cm^{-1} were correlated to the stretching of the aliphatic methyl group in 2-MIM, C=N stretching in 2-MIM, stretching and bending of the imidazole ring and the Co-N stretching for ZIF-67 and Zn-N for ZIF-8 [41]. These findings not only confirmed the introduction of carboxylate groups on the surface of the nanocellulose fibers, but also a change in the chemical environment of the carboxylate groups after the sodium ion was exchanged with either Co^{2+} or Zn^{2+} after addition of metal salts. Due to the fact that ZIF-8 is isostructural to ZIF-67 and is composed of the same constituents, excluding zinc ions instead of cobalt, the FTIR spectra were rather similar, also confirming the presence of ZIF-8 on the TEMPO-CNFs.

The images presented in Figure 11 are SEM micrographs of nanopaper composed of pure *Cladophora* cellulose which had endured 6 hours of TEMPO-mediated oxidation. As mentioned in previous sections, during the oxidation, -OH groups at C6 were selectively oxidized into sodium carboxylate groups, essentially depolymerizing and inhibiting formation of hydrogen bonds between adjacent chains, rendering the polymer with long, individualized and thinner fibers instead [42]. As can be seen in the figure, the individualized nanofibrils are clearly visible as a direct result of the TEMPO-oxidation.

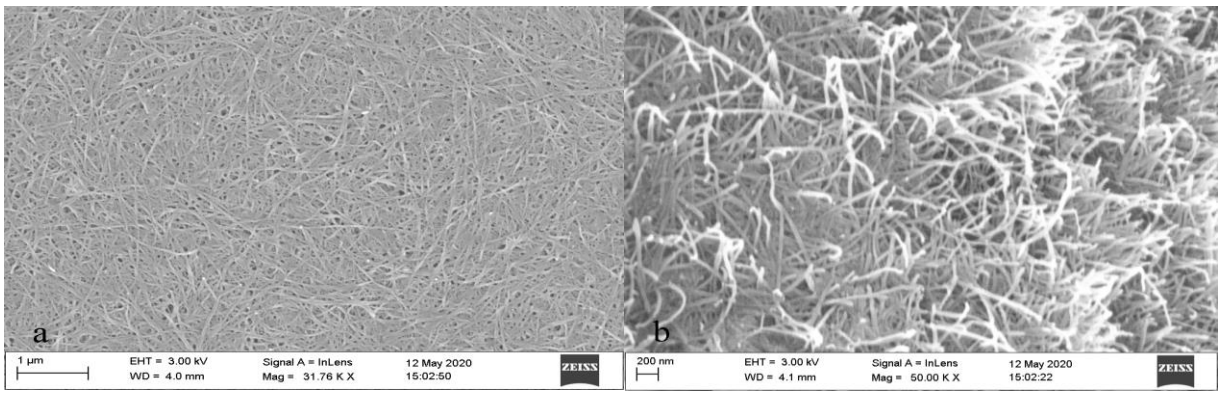

Figure 11. (a) Pure TEMPO-CNFs seen from above**. (b)** TEMPO-CNFs at a higher magnification. Notice the individualized fibers as a direct result from oxidation**.**

Unfortunately, the SEM micrographs of the CNF@ZIFs nanocomposites were difficult to obtain, many of them were perceived to be blurry to be able to distinguish direct, in-depth, results from. The reason is speculated to be due to poor conductivity between the substrate used for SEM imaging and the freestanding nanopapers. Thus, those that were deemed acceptable to draw any conclusion from were selected and are presented in Figure 12.

Figure 12(a-c) depicts the CNF@ZIF-8 nanofibers with different metal salt concentrations used during synthesis. At first glance, the surfaces for all the nanocomposites were somewhat reminiscent of pure TEMPO-CNFs. Although, the inset images which depict magnified versions of the respective micrographs showcased that there were clear and distinct crystals which were distributed in an assembled manner along the individual nanocellulose fibers. This signified not only successful formation of ZIF-8 crystals, but also successful attachment of these crystals along the outer surface of the nanofibrils. Although, for the CNF@ZIF-8:A2, there seemed to be a coalesced layer instead of individual nanoparticles. This coalesced layer made it very hard to determine whether there were individually wrapped ZIF-8 layers on the nanocellulose fibers or not. A viable reason for the formed layer may have been due to heavy amounts of remaining organic solvent.

Inspecting the surface, it seemed rather rough, and some ZIF-8 particle agglomeration could be seen distributed in random locations for all CNF@ZIF-8 samples which may have pointed toward an insufficient washing after the ion-exchange, leading to a higher accumulation of metal ions than the calculated amount, thus, allowing formation for excess ZIF-8 crystals. Compared to CNF@ZIF-8 nanocomposites, the CNF@ZIF-67 nanocomposites were deemed to have obtained a much smoother surface with less agglomerated crystal particles. Although, the inhomogeneity

throughout the papers, in regard to ZIFs morphology, seemed to be a reoccurring trait; CNF@ZIF-67 exhibited an overall varied fibril thickness, especially CNF@ZIF-67:B2, as can be seen in Figure 12e. The smooth surface may be explained by the fact that the majority of free particles have been removed by the multiple washings, diminishing the occlusion of CNF@ZIF-67 hybrid nanofibrils in the micrographs. For CNF@ZIF-67:A2, the overall morphology was that of a layered structure and partially agglomerated spherical particles at random locations. The difference

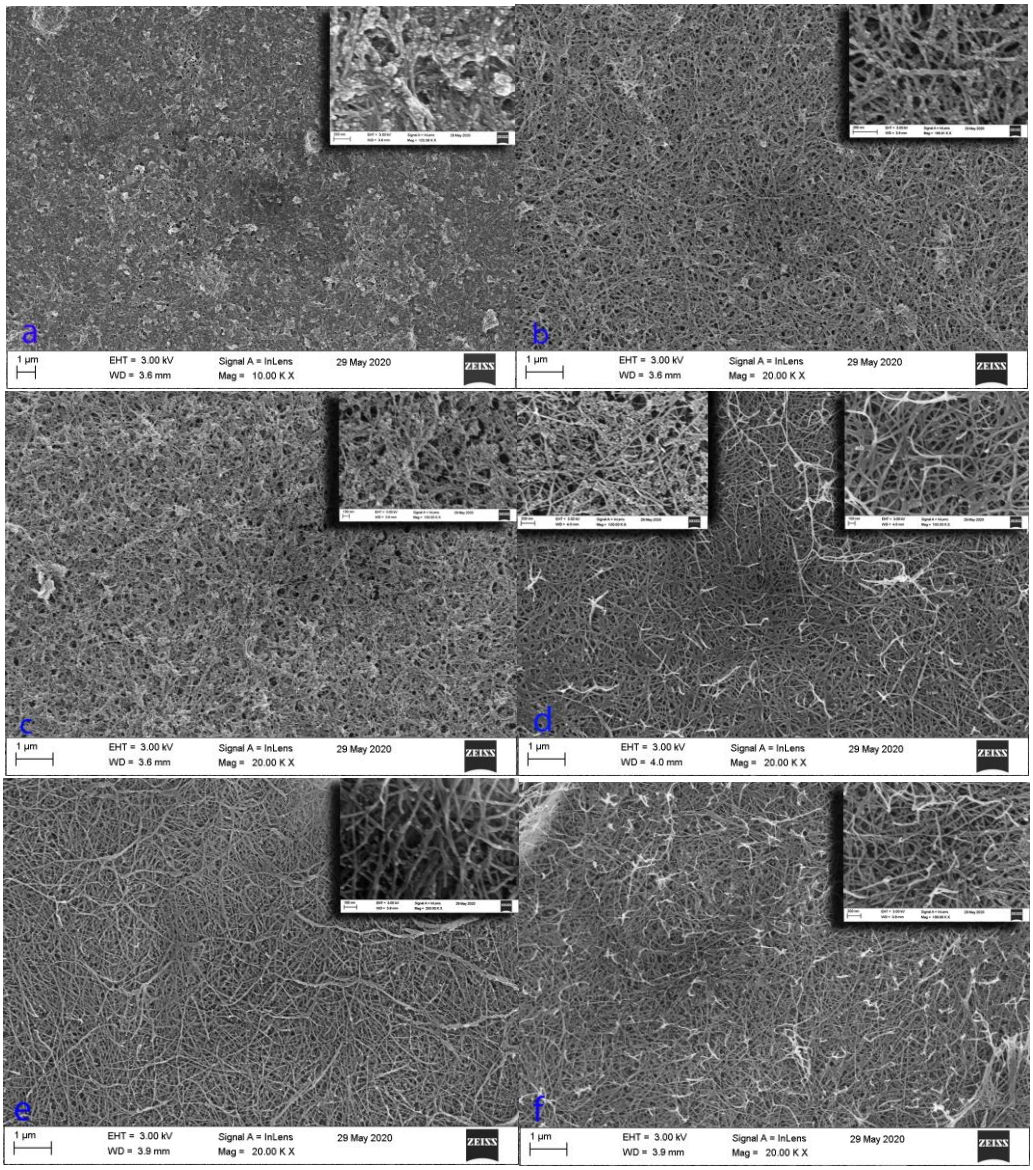

Figure 12. (a-c) CNF@ZIF-8:A2, B2 and C2**. (d-f)** CNF@ZIF-67:A2, B2 and C2**.**

in the morphologies of both nanocomposites, despite the same washing steps, indicates that ZIF-67 crystals seem to be easier to wash away than ZIF-8. Another reason for the low amount of spherical particles may be that ZIF-67 crystals under conditions given, perhaps favored the layered morphology over the spherical, agglomerated morphology.

Pure TEMPO-CNFs has a typical fiber diameter of ~25-30 nm as mentioned in Section 2.1. Although, the fibers of CNF@ZIFs nanocomposite which could be roughly measured, without spherical particles in the way or too much a blurriness in the micrograph, had diameters ranging from ~32-47 nm suggesting successful growth of ZIF-crystal with layered morphology had been achieved at random locations in all the samples. The only exception being CNF@ZIF-8:A2 due to the coalesced layer which made measuring impossible. In essence, all the samples did have areas of inhomogeneity where spherical morphology of ZIF crystals could be observed to a certain degree. The fact that there was inhomogeneity throughout the samples with mixed morphologies made it difficult to determine whether there was an increase in probability of gaining layered morphologies for an increased metal salt concentration. The relation was deemed to be random.

4.3.2 Thermal analysis of CNF@ZIFs nanocomposites

As can be seen from the TGA analysis in Figure 13, the initial thermal degradation, T_d, of TEMPO-CNFs occurred at ~245^o C. The initial T_d for the CNF@ZIFs nanocomposites, corresponding to the degradation of the TEMPO-CNFs component due to pyrolysis, occurred directly at ~324^o C for CNF@ZIF-67 nanocomposites and ~330^o C for CNF@ZIF-8 nanocomposites. Furthermore, the major mass loss of TEMPO-CNFs was significantly lowered in the nanocomposites, especially for CNF@ZIF-8. It is known that pristine ZIF-67 has a lower thermal stability than pristine ZIF-8, which explained the difference in their ability to protect the TEMPO-CNFs from degradation in the CNF@ZIF-67- and CNF@ZIF-8 nanocomposites [43]. The mass loss occurring from 0-100^o C for pure TEMPO-CNFs is attributed to be due to water evaporation.

These observations support the SEM findings that there should have been formation of core-shell structure between the TEMPO-CNFs and ZIFs with the layered morphology, at least to some extent, as Zhou et al observed the same trend in their CNF@MOFs with continuous, homogenous layers of MOF crystals [17]. As was commented on the SEM micrographs, this layered morphology might not have been the case fully throughout the samples. From what could be observed, the morphology of the ZIF crystals were a mix between reoccurring spherical particles and core-shell structure. Interestingly, a trend in the TGA curves could be observed for each of the nanocomposites. Also, the major weight loss seen for the TEMPO-CNFs was further inhibited as the metal salt increased during synthesis of CNF@ZIF.

Also, it could be speculated that obtaining mixed morphologies of ZIF crystals growing upon the TEMPO-CNFs may be sufficient to induce a thermal barrier strong enough to decrease the degradation of the cellulose fibers as a whole. Simultaneously, the trend emphasized that a higher amount of metal salt yielded a higher loading of ZIFs within the nanocomposite. Thus, a higher loading of ZIFs incorporated an increased thermal protection to the TEMPO-CNFs component. Nonetheless, these results indicated that the nanocomposites are viable for various endeavors in room temperature and perhaps flue gas treatments, where temperature ranges are

within ~47-127^{o} C, without risking severe thermal decomposition [44]. Corresponding DTG curve may be seen in Figure F3 in the Appendix.

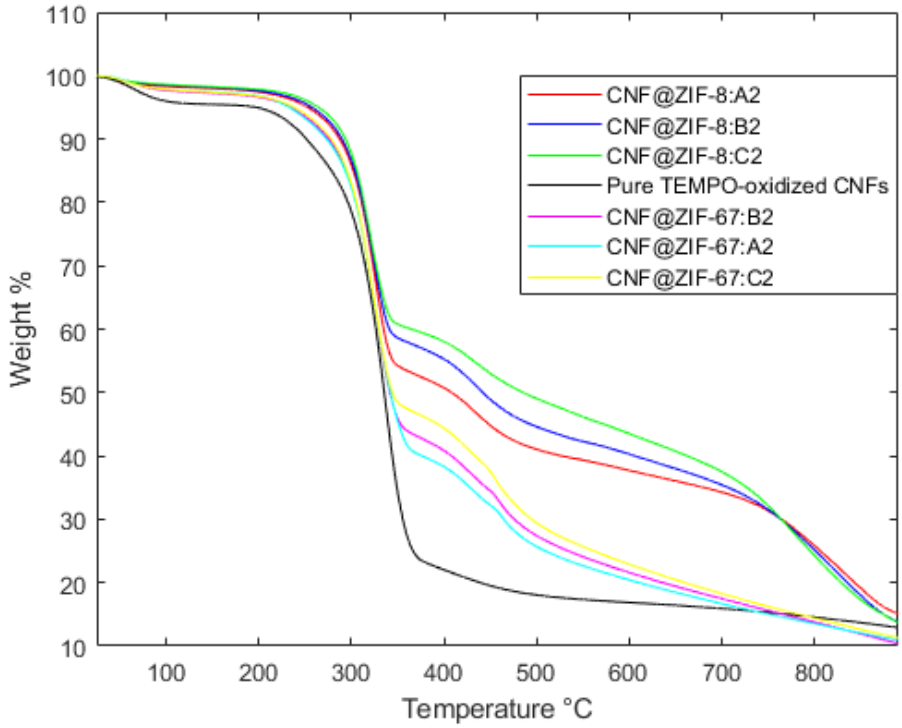

Figure 13. TGA curve for pure TEMPO-oxidized CNFs and CNF@ZIF-8/CNF@ZIF-67 with varying amounts of Zn/Co-salt used during synthesis**.**

4.3.3 Porosity analysis of CNF@ZIFs nanocomposites

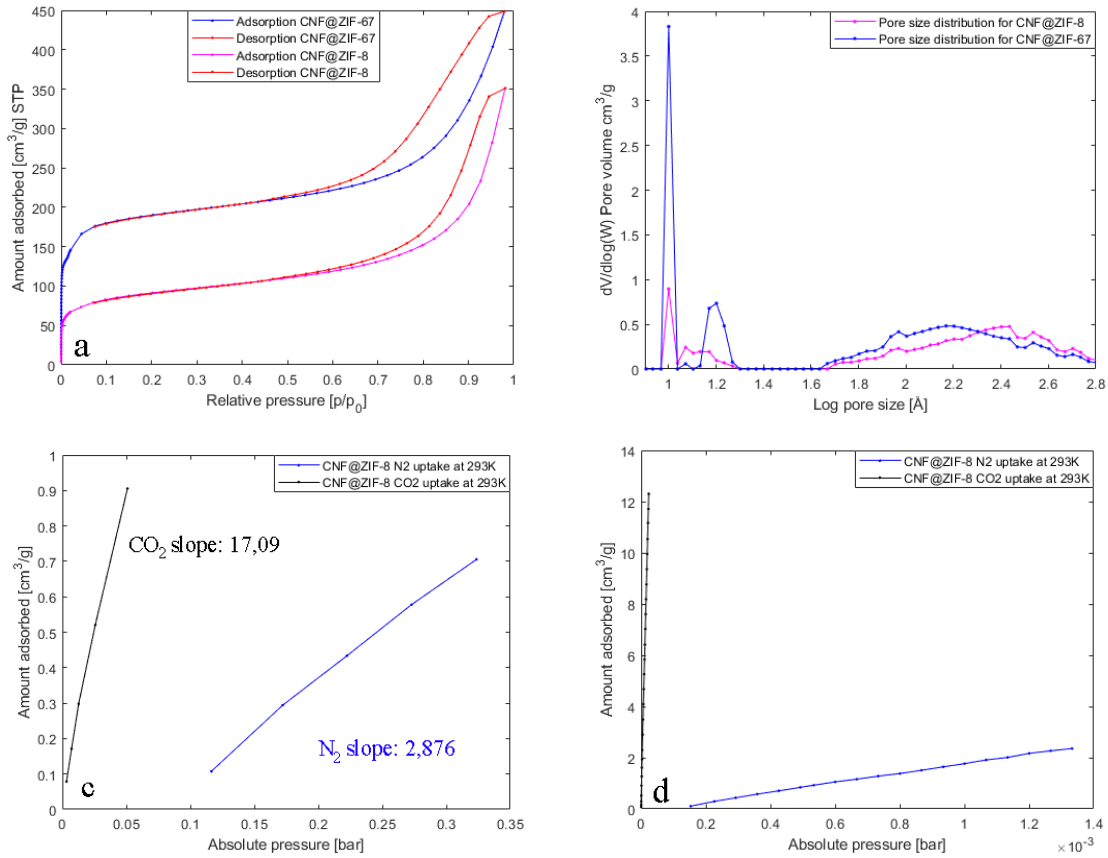

Figure 14. (a) N_2-sorption isotherms of both nanocomposites at 77 K, showcasing the mesoporous nature**. (b)** DFT derived pore size distribution with logarithmic x-axis**. (c)** The Henry's law selectivity initial slopes of CNF@ZIF-8 at 293K for CO_2 and N_2, respectively**. (d)** Isotherms obtained at 293 K for scaled-up CNF@ZIF-8.

The results obtained from N_2 gas sorption measurements may be observed in Figure 14 and represented the analysis of the scaled-up nanocomposite papers of CNF@ZIFs. Both of them exhibited an isotherm which was deemed to belong to a mix between micro- and mesoporous materials and can be seen in Figure 14a [35]. This was expected as the substrate component of the composites was TEMPO-CNFs, which is known to retain a fibrous, intertwined network and has been demonstrated to retain a mesoporous structure. Seemingly, at very low relative pressures a steep increase of adsorbate was observed which could be attributed to the quick filling of microporous ZIF crystals. The steady but slow increase of adsorbate uptake beyond this point was due to multilayers forming on the surface of the mesopores until the they had been completely filled. During desorption a clear hysteresis loop could be noticed being formed which was attributed to capillary condensation; yet another characteristic trait related to mesoporous

materials. These findings indicated a hierarchical porous structure, thanks to the synergetic effects of microporous ZIFs and mesoporous TEMPO-CNFs.

The DFT pore size distribution, which depicted the pore volume of the nanocomposite as a function of the abundance of a certain pore width, can also be seen in Figure 14b. Notice that the x-axis was set to logarithmic scale to allow proper observation of the whole distribution range. The majority of the pore volume for both nanocomposites was comprised of a wide range of pores which had a width larger than ~2 nm, further confirming the mesoporosity of both materials. Although, pores with sizes ranging from ~1-2 nm could be distinguished in the microporous region. These pores had sizes matching that of microporous materials, hence it could be deduced that these correlated to the pores of ZIF crystals, which is in accordance with previous reports [45]. The pore size which occurred the most within the microporous region of both nanocomposites was similar, ~1nm, which is consistent with the pore size of ZIF-67 and ZIF-8 synthesized in MeOH. Interestingly, there was a slight difference in the overall pore size distribution between the two CNF@ZIFs. This may be attributed to inherently different morphologies between the nanocomposites.

The BET surface area is presented in Table 3 and as can be seen, the surface area for both CNF@ZIF-67 and CNF@ZIF-8 was superior than for pure TEMPO-CNFs (BET specific surface area ~100 m^2/g), especially the CNF@ZIF-67 with a remarkable BET surface area of ~686 m^2/g [46]. This finding was logical, the total BET surface area of the nanocellulose substrate should have been enhanced due to the contribution given by microporous ZIF crystals grown upon them, as pristine ZIFs are known to retain substantially high surface areas, as mentioned in Section 2.6.

The CO_2-over-N_2 selectivity for CNF@ZIF-8 at 293K was also calculated using *Henry´s law selectivity* via initial slope calculations and may be seen in Figure 14c [47]. This is a simple and formally exact approach to calculate the CO_2 selectivity of mixed gases using single-component isotherms. That is; obtaining isotherms for N_2- and CO_2 gas separately and calculate the slope of the respective isotherms at low pressures and obtain the ratio between the slopes. The reason as to why the slope should be calculated at lower pressures at 293K is due to the fact that flue gas treatments may occur in these low-pressure conditions [48]. These conditions are often called the flue gas treatment regime in the industry. Thus, deriving the slope of the isotherms at low pressures allowed for an estimate on how well the selectivity towards CO_2 the hierarchically porous materials were, contra N_2 in a potential gas mixture during flue gas treatment.

The initial slope of the isotherm correlated to the adsorption of CO_2 was much steeper than for N_2 which showcased the higher rate of CO_2 uptake at lower pressures. The ratio between the slopes was calculated to ~6 and hereby a proof-of-concept of CNF@ZIF-8 to act as a filter membrane for selective CO_2 removal in a CO_2/N_2-gas mixture was visualized. Unfortunately, the CO_2-over-N_2 selectivity of CNF@ZIF-67 was never calculated due to time limitation. The effect of pore size was also studied by Yaghi et al [26] and no noticeable differences were found between ZIFs with different pore sizes and CO_2-selectivity, rather the chemical affinity due to the polar functional groups and different metal ions seemed to be the dominating factor over

selectivity. For instance, ZIF-67 was reported to showcase an even better CO_2-selectivity than ZIF-8, which affirms that CNF@ZIF-67 should have CO_2-selectivity too.

From Figure 13d, a clear difference could be observed for the uptake of respective gases at similar pressures. CO_2 was abundantly adsorbed at lower pressures, whereas N_2 uptake slightly increased over the whole pressure range. This further suggests that the CNF@ZIFs are viable candidates as filter membranes for effective uptake of CO_2 within flue gas regimes.

Table 3. Properties of nanocomposites vs pure TEMPO-CNFs related to their porosities**.**

	S_{BET} [m^2/g]	**CO_2/N_2**
CNF@ZIF-67	~687	-
CNF@ZIF-8	~325	~6
Pure TEMPO-CNFs	~100	-

5. Conclusions

In this master's thesis, experiments were conducted in order to try and synthesize hybrid nanocomposites of CNF@ZIF-8 and CNF@ZIF-67 by an interfacial synthesis approach. The results presented in previous sections proved the successful synthesis and in-situ growth of ZIFs nanocrystals in ambient conditions upon TEMPO-CNFs. Furthermore, success in forming flexible and shapeable CNF@ZIF paper membranes with potential industrial applications as selective CO_2 filter membranes for flue gas treatment was achieved. The concept behind the interfacial synthesis approach was to grow ZIF crystals upon nanocellulose fiber surfaces which had undergone carboxylation thanks to a TEMPO-mediated oxidation. This allowed for ion-exchanging with metal ions corresponding to those which respective ZIF is composed of. By adding organic linkers and a further amount of metal ions, the framework was successfully grown upon the nanocellulose surface. By increasing the metal ion concentration, a series of analytical measurements were conducted to observe the morphological change of the crystals surrounding the nanocellulose fibers and how it affected the composites.

XRD measurements performed for pure TEMPO-oxidized nanocellulose, pure ZIFs and CNF@ZIFs nanocomposites suggests successful incorporation of ZIFs in the TEMPO CNFs. Further analysis with FTIR points towards successful TEMPO-oxidation due to introduction of absorption band at ~1612 cm^{-1} for TEMPO-oxidized cellulose compared to pure Cladophora cellulose. Additionally, ion-exchange resulted in a shifting of this peak for CNF@ZIFs. Furthermore, characteristic ZIFs peaks could be observed which indicated that incorporation of ZIFs on the TEMPO-CNF had been achieved.

SEM micrographs were also obtained to observe growth of ZIFs and morphological changes with increased metal salts used in the synthesis of CNF@ZIFs. A partially continuous core-shell

morphology could be seen. The morphologies ranged from spherical- and/or interconnected layered crystals forming the core-shell structure with the cellulose fibers. The thickness of measurable CNF@ZIFs layers in CNF@ZIF-67 and CNF@ZIF-8 ranged from ~32-47 nm, which is larger than the diameter of pure CNFs (~25-30 nm). No concise relation between the amount of metal salt used and the probability of gaining a core-shell structure could be drawn. TGA analysis revealed enhanced thermal stability of the TEMPO-CNFs component due to protective contribution from the partially layered ZIFs. An increased amount of metal salt used during synthesis resulted in a decrease of TEMPO-CNFs mass loss, seemingly independent from obtained morphologies.

The BET surface area of the CNF@ZIF-8 and CNF@ZIF-67 nanopapers were superior to pure TEMPO-CNFs nanopapers with values of ~325 m^2/g and ~687 m^2/g respectively versus ~100 m^2/g.

Finally, a proof-of-concept was shown by performing CO_2/N_2-sorption measurements at 293 K on the scaled-up CNF@ZIF-8 nanopaper. By calculating the Henry's law selectivity ratio of the initial slopes for the isotherms obtained in N_2 and CO_2 at 293 K it was proven that CNF@ZIF-8 preferred adsorbing CO_2 over N_2. Also, the CO_2 uptake at 293 K was superior at low pressures, compared to N_2 uptake.

6. Future perspectives

As was mentioned in Section 4.1 the solvent-exchange procedure hampered a lot with the experiments due to the fact that the amount of available cellulose diminished with each cycle. The first few tries yielded poor to mediocre results. The papers obtained where brittle due to the abundance of pure ZIF crystals compared to the little amount nanocellulose. Further increasing the cellulose amount yielded better and shapeable papers, although calibrating the concentration of the final TEMPO-CNFs solution after solvent-exchange is crucial to determine the amount of final cellulose mass for future references and lower the risk of brittle/too thin papers without the necessity of performing repeated experiments. In order to further diminish this loss, using vacuum filtration and then collecting the filter cake may be a better alternative to think about in the future.

The SEM images from Section 4.3.1 showcased the morphology of the grown ZIF crystals for each nanocomposite. It may be concluded that the morphology was unfortunately not very continuous throughout the samples, as both spherical and partially layered structures were found with variation in thickness in the ZIF layers. Albeit, this did not seem to affect the loading of the ZIFs in the composites as was mentioned and reflected in the obtained TGA curves. Although, morphological control and achieving continuous layers would be beneficial as a denser amount of ZIFs would be obtained if continuous hybrid layers are formed.

Even though the BET surface area of both nanocomposites was superior compared to pure TEMPO-CNFs it would be interesting to try and correlate the difference between ZIF morphologies and the BET surface area of the composites. Having a continuous layer of densely packed ZIFs on the TEMPO-CNFs with high coverage should inherently maximize the BET

surface area of the composite and allow for a higher uptake of gas. Preferably, performing the N_2-sorption tests on all the nanocomposites would have been optimal in order to be able to compare the morphologies and ZIF loading to the isotherms and see how the increased amount of metal ions would impact properties related to the porosity. Unfortunately, due to time limitations only one of each CNF@ZIFs nanocomposites was scaled-up for gas sorption measurements.

As pointed out in Section 3, all the experiments were conducted in MeOH as solvent. The reason being that it had been shown that 2-MIM deprotonates with sufficient rate in MeOH to successfully form ZIFs. Although, MeOH is toxic to humans and scaling up with this solvent for industrial production of the nanocomposites might not be sustainable in the long run. Thus, another greener solvent should be implemented during synthesis. It has been reported that ZIFs have been synthesized in aqueous conditions via room temperature methods, yielding crystalline ZIFs without additives, albeit; a much higher amount of organic ligands would be needed to facilitate the formation of the framework structure and form nanoparticles in water [49]. At low amounts of 2-MIM, the resulting compound would be either hydroxylated metal ions or unknown hydroxylated complexes rather than pure-phase ZIFs. It could be speculated that the deprotonation rate in water for 2-MIM is much slower compared to in MeOH because of solvent-solute interactions. Hence, allowing time for generation of unwanted products rather than ZIFs. Furthermore, a very high amount of linker may not be financially sustainable if CNF@ZIF nanocomposites were to be synthesized and scaled up. With addition of TEA, the deprotonation rate is most probably facilitated in aqueous conditions and favor the formation of crystalline pure-phase ZIF nanoparticles over hydroxylated metal ions. [30, 50]. Thus, addition of a deprotonating agent to facilitate the deprotonation of 2-MIM in water might increase the probability of successful ZIF formation. In summary, taking solute-solute vs. solute-solvent interactions into consideration might be of relevance. Performing synthesis in water would also greatly impede the loss of TEMPO-CNFs, as solvent-exchange would not be necessary.

Taking the charge density of the sodium carboxylates on the TEMPO-CNFs into consideration would also be beneficial. Increasing the charge density effectively yields more sites for ion-exchange, favoring the formation of densely packed ZIFs crystals on the surface. Thus, performing the TEMPO-mediated oxidation for prolonged periods of time might be a relevant parameter to take into consideration for future references. Furthermore, abundant amounts of anchoring sites should facilitate and further promote the interconnected, layered, morphology of the ZIFs.

7. Bibliography

1. WHO | WHO Global Ambient Air Quality Database (update 2018). In: WHO. http://www.who.int/airpollution/data/cities/en/. Accessed 15 Jun 2020

2. Izatt RM (2016) Macrocyclic and Supramolecular Chemistry: How Izatt-Christensen Award Winners Shaped the Field. John Wiley & Sons

3. Huang X, Zheng B, Liu Z, et al (2014) Coating Two-Dimensional Nanomaterials with Metal–Organic Frameworks. ACS Nano 8:8695–8701. https://doi.org/10.1021/nn503834u

4. Zhu L, Zong L, Wu X, et al (2018) Shapeable Fibrous Aerogels of Metal–Organic-Frameworks Templated with Nanocellulose for Rapid and Large-Capacity Adsorption. ACS Nano 12:4462–4468. https://doi.org/10.1021/acsnano.8b00566

5. Pihl L, Svensson A (2001) Biologisk undersökning av grunda havsvikar: effekter av fintrådiga alger och skörd. Länsstyrelsen i Västra Götalands län

6. Klemm D, Heublein B, Fink H-P, Bohn A (2005) Cellulose: Fascinating Biopolymer and Sustainable Raw Material. Angew Chem Int Ed 44:3358–3393. https://doi.org/10.1002/anie.200460587

7. Ansell MP, Mwaikambo LY (2009) The structure of cotton and other plant fibres. In: Handbook of Textile Fibre Structure. Elsevier, pp 62–94

8. Mihranyan A (2011) Cellulose from cladophorales green algae: From environmental problem to high-tech composite materials. J Appl Polym Sci 119:2449–2460. https://doi.org/10.1002/app.32959

9. Chinga-Carrasco G (2011) Cellulose fibres, nanofibrils and microfibrils: The morphological sequence of MFC components from a plant physiology and fibre technology point of view. Nanoscale Res Lett 6:417. https://doi.org/10.1186/1556-276X-6-417

10. Lee K-Y (2018) Nanocellulose and Sustainability: Production, Properties, Applications, and Case Studies. CRC Press

11. Saito T, Hirota M, Tamura N, et al (2009) Individualization of Nano-Sized Plant Cellulose Fibrils by Direct Surface Carboxylation Using TEMPO Catalyst under Neutral Conditions. Biomacromolecules 10:1992–1996. https://doi.org/10.1021/bm900414t

12. Pierre G, Punta C, Delattre C, et al (2017) TEMPO-mediated oxidation of polysaccharides: An ongoing story. Carbohydr Polym 165:71–85. https://doi.org/10.1016/j.carbpol.2017.02.028

13. Park J, Park C-W, Han S-Y, et al (2019) Effects of pH on Nanofibrillation of TEMPO-Oxidized Paper Mulberry Bast Fibers. Polymers 11:414. https://doi.org/10.3390/polym11030414

14. Saito T, Isogai A (2005) Ion-exchange behavior of carboxylate groups in fibrous cellulose oxidized by the TEMPO-mediated system. Carbohydr Polym 61:183–190. https://doi.org/10.1016/j.carbpol.2005.04.009

15. Zhu H, Yang X, Cranston ED, Zhu S (2016) Flexible and Porous Nanocellulose Aerogels with High Loadings of Metal–Organic-Framework Particles for Separations Applications. Adv Mater 28:7652–7657. https://doi.org/10.1002/adma.201601351

16. Koczkur KM, Mourdikoudis S, Polavarapu L, Skrabalak SE (2015) Polyvinylpyrrolidone (PVP) in nanoparticle synthesis. Dalton Trans 44:17883–17905. https://doi.org/10.1039/C5DT02964C

17. Zhou S, Strømme M, Xu C (2019) Highly Transparent, Flexible, and Mechanically Strong Nanopapers of Cellulose Nanofibers @Metal–Organic Frameworks. Chem – Eur J 25:3515–3520. https://doi.org/10.1002/chem.201806417

18. Soni S, Bajpai P, Arora C (2018) A review on metal-organic framework: synthesis, properties and application. Charact Appl Nanomater 2:. https://doi.org/10.24294/can.v2i2.551

19. Banerjee D, Wang H, Deibert BJ, Li J (2016) Alkaline Earth Metal-Based Metal–Organic Frameworks: Synthesis, Properties, and Applications. In: The Chemistry of Metal–Organic Frameworks. John Wiley & Sons, Ltd, pp 73–103

20. Reticular Chemistry in All Dimensions | ACS Central Science. https://pubs.acs.org/doi/10.1021/acscentsci.9b00750. Accessed 15 Jun 2020

21. Abbasloo F, Khosravani SA, Ghaedi M, et al (2018) Sonochemical-solvothermal synthesis of guanine embedded copper based metal-organic framework (MOF) and its effect on oprD gene expression in clinical and standard strains of Pseudomonas aeruginosa. Ultrason Sonochem 42:237–243. https://doi.org/10.1016/j.ultsonch.2017.11.035

22. Tranchemontagne DJ, Hunt JR, Yaghi OM (2008) Room temperature synthesis of metal-organic frameworks: MOF-5, MOF-74, MOF-177, MOF-199, and IRMOF-0. Tetrahedron 64:8553–8557. https://doi.org/10.1016/j.tet.2008.06.036

23. Park KS, Ni Z, Cote AP, et al (2006) Exceptional chemical and thermal stability of zeolitic imidazolate frameworks. Proc Natl Acad Sci 103:10186–10191. https://doi.org/10.1073/pnas.0602439103

24. Ghosh SK, Kitagawa S (2019) Introduction. In: Metal-Organic Frameworks (MOFs) for Environmental Applications. Elsevier, pp 1–4

25. (PDF) Zeolites and MOFs: what they are and their use in sensing applications. In: ResearchGate. https://www.researchgate.net/publication/308953659_Zeolites_and_MOFs_what_they_are_and_their_use_in_sensing_applications. Accessed 16 Jun 2020

26. Phan A, Doonan CJ, Uribe-Romo FJ, et al (2010) Synthesis, Structure, and Carbon Dioxide Capture Properties of Zeolitic Imidazolate Frameworks. Acc Chem Res 43:58–67. https://doi.org/10.1021/ar900116g

27. Wang M, Liu J, Guo C, et al (2018) Metal–organic frameworks (ZIF-67) as efficient cocatalysts for photocatalytic reduction of CO_2 : the role of the morphology effect. J Mater Chem A 6:4768–4775. https://doi.org/10.1039/C8TA00154E

28. Zhang H, Zhao M, Yang Y, Lin YS (2019) Hydrolysis and condensation of ZIF-8 in water. Microporous Mesoporous Mater 288:109568. https://doi.org/10.1016/j.micromeso.2019.109568

29. Canivet J, Fateeva A, Guo Y, et al (2014) Water adsorption in MOFs: fundamentals and applications. Chem Soc Rev 43:5594–5617. https://doi.org/10.1039/C4CS00078A

30. Md. Nordin NAH, Ismail A, Mustafa AB, et al (2014) Aqueous room temperature synthesis of zeolitic imidazole framework 8 (ZIF-8) with various concentrations of triethylamine. RSC Adv 4:33292–33300. https://doi.org/10.1039/C4RA03593C

31. Biopolymer@Metal-Organic Framework Hybrid Materials_ A Critical Survey | Elsevier Enhanced Reader. https://reader.elsevier.com/reader/sd/pii/S0079642519300611?token=323296A287B6B8BE1ACBF5CE9769F06BA6384F52C0CCBDB5AEC3E3EE5309E53D497FC8E7BE4D1A178C3C33538BBF356C. Accessed 16 Jun 2020

32. Laurila E, Thunberg J, Argent SP, et al (2015) Enhanced Synthesis of Metal-Organic Frameworks on the Surface of Electrospun Cellulose Nanofibers: Enhanced Synthesis of Metal-Organic Frameworks. Adv Eng Mater 17:1282–1286. https://doi.org/10.1002/adem.201400565

33. Park J, Oh M (2017) Construction of flexible metal–organic framework (MOF) papers through MOF growth on filter paper and their selective dye capture. Nanoscale 9:12850–12854. https://doi.org/10.1039/C7NR04113F

34. Matsumoto M, Kitaoka T (2016) Ultraselective Gas Separation by Nanoporous Metal−Organic Frameworks Embedded in Gas-Barrier Nanocellulose Films. Adv Mater 28:1765–1769. https://doi.org/10.1002/adma.201504784

35. Sotomayor FJ, Cychosz KA, Thommes M (2018) Characterization of Micro/Mesoporous Materials by Physisorption: Concepts and Case Studies. 17

36. Universiti Sains Malaysia, Peng Chee T, Boon Seng O, et al (2017) Size Control and Stability Study of Zeolitic Imidazolate Framework-8 to Prepare Mixed Matrix Membrane. J Phys Sci 28:215–226. https://doi.org/10.21315/jps2017.28.s1.14

37. Qian L, Lei D, Duan X, et al (2018) Design and preparation of metal-organic framework papers with enhanced mechanical properties and good antibacterial capacity. Carbohydr Polym 192:44–51. https://doi.org/10.1016/j.carbpol.2018.03.049

38. Qian R, Tang A, Chen G (2011) TEMPO-Mediated Oxidation of Cellulose and Preparation of Cellulose Nanofibrils. J Biobased Mater Bioenergy 5:253–257. https://doi.org/10.1166/jbmb.2011.1145

39. Jiao L, Bian H, Gao Y, et al (2018) Highly Dispersible Cellulose Nanofibrils Produced via Mechanical Pretreatment and TEMPO-mediated Oxidation. Fibers Polym 19:2237–2244. https://doi.org/10.1007/s12221-018-8565-5

40. Zhou S, Apostolopoulou-Kalkavoura V, Tavares da Costa MV, et al (2020) Elastic Aerogels of Cellulose Nanofibers@Metal–Organic Frameworks for Thermal Insulation and Fire Retardancy. Nano-Micro Lett 12:9. https://doi.org/10.1007/s40820-019-0343-4

41. Verpoort F, Mousavi B, Zanon A, Chaemchuen S (2017) Zn-doped ZIF-67 as catalyst for the CO2 fixation into cyclic carbonates. J CO2 Util Volume 20:Pages 282–291. https://doi.org/10.1016/j.jcou.2017.05.026

42. Isogai A, Hänninen T, Fujisawa S, Saito T (2018) Review: Catalytic oxidation of cellulose with nitroxyl radicals under aqueous conditions. Prog Polym Sci 86:122–148. https://doi.org/10.1016/j.progpolymsci.2018.07.007

43. Sun W, Zhai X, Zhao L (2016) Synthesis of ZIF-8 and ZIF-67 nanocrystals with well-controllable size distribution through reverse microemulsions. Chem Eng J 289:59–64. https://doi.org/10.1016/j.cej.2015.12.076

44. Songolzadeh M, Soleimani M, Takht Ravanchi M, Songolzadeh R (2014) Carbon Dioxide Separation from Flue Gases: A Technological Review Emphasizing Reduction in Greenhouse Gas Emissions. In: Sci. World J. https://www.hindawi.com/journals/tswj/2014/828131/. Accessed 25 Jun 2020

45. Zhou K, Mousavi B, Luo Z, et al (2017) Characterization and properties of Zn/Co zeolitic imidazolate frameworks vs. ZIF-8 and ZIF-67. J Mater Chem A 5:952–957. https://doi.org/10.1039/C6TA07860E

46. Zhou S, Nyholm L, Strømme M, Wang Z (2019) *Cladophora* Cellulose: Unique Biopolymer Nanofibrils for Emerging Energy, Environmental, and Life Science Applications. Acc Chem Res 52:2232–2243. https://doi.org/10.1021/acs.accounts.9b00215

47. Li G, Zhang B, Yan J, Wang Z Electronic Supplementary Information. 10

48. Mecerreyes D (2015) Applications of Ionic Liquids in Polymer Science and Technology. Springer

49. (PDF) Water-based synthesis of zeolitic imidazolate framework-8 for CO 2 capture. https://www.researchgate.net/publication/317351929_Water-based_synthesis_of_zeolitic_imidazolate_framework-8_for_CO_2_capture. Accessed 8 Jul 2020

50. Mostafazadeh N, Ghoreyshi AA, Pirzadeh K (2018) Optimization of Solvothermally Synthesized ZIF-67 Metal Organic Framework and Its Application for Cr (VI) Adsorption from Aqueous Solution. Adsorpt Aqueous Solut 15:21

51. Feng X, Wu T, Carreon MA (2016) Synthesis of ZIF-67 and ZIF-8 crystals using DMSO (Dimethyl Sulfoxide) as solvent and kinetic transformation studies. J Cryst Growth 455:152–156. https://doi.org/10.1016/j.jcrysgro.2016.10.016

8. Appendix

Table A1. Details over reagents used for initial experiments conducted by the 1-step process for synthesis of CNF@ZIF-67**.** The low amount of CNFs is due to a wrongly calibrated TEMPO-CNFs batch and the molar ratio metal-ligand was 1:10**.**

$Co(NO_3)_2 \cdot 6H_2O$ (mg)	**TEA (µL)**	**2-MIM (mg)**	**PVP (mg)**	**CNFs (mg)**	**Definition**
15	72	42	10	12,3	CNF@ZIF-67:A1
20	96	56	10	12,3	CNF@ZIF-67:B1
25	119	70	10	12,3	CNF@ZIF-67:C1

Figure F1. (a) CNF@ZIF-67:A1. **(b)** CNF@ZIF-67:B1**. (c)** CNF@ZIF-67:C1. Notice the abundant, spherical, ZIF-67 nanoparticles present both around and on the nanocellulose fibers due to the lack of washing after the ion-exchange. Severe agglomeration of ZIF-67 particles may also be observed at certain locations, especially for CNF@ZIF-67:C1**.**

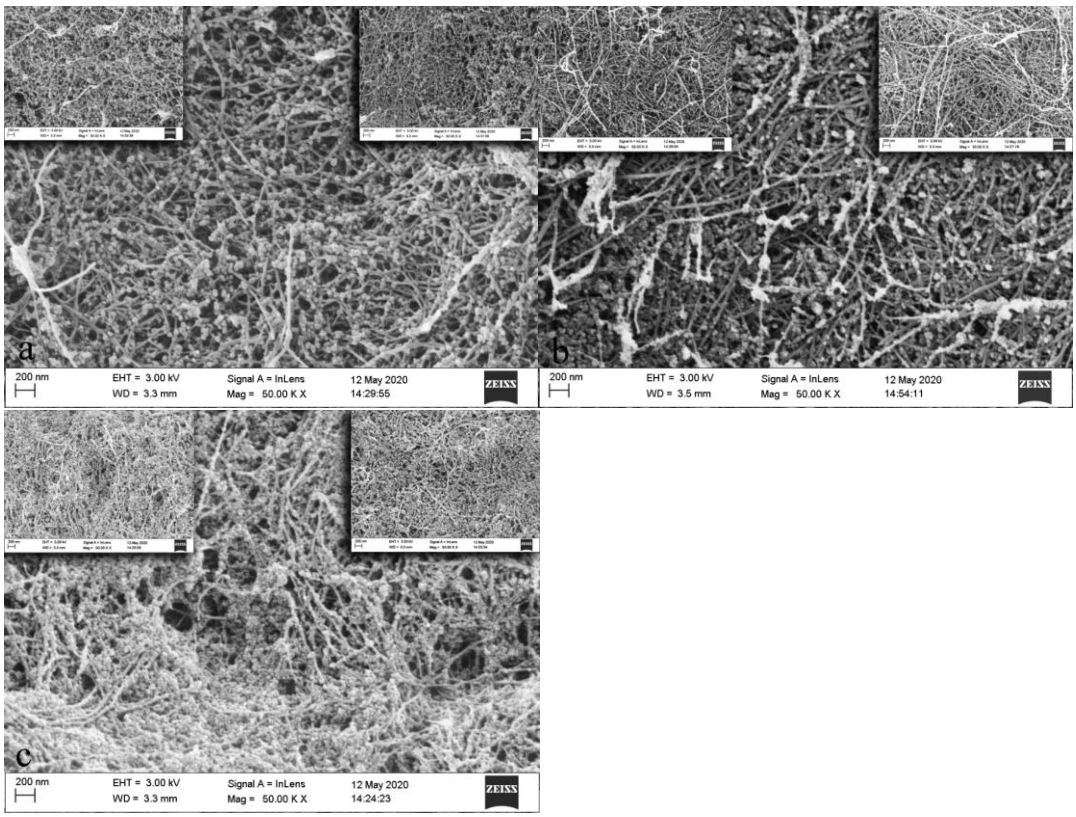

Figure F2. (a) Failed CNF@ZIF-67 solution**. (b)** Successful CNF@ZIF-67 solution**. (c)** Successful CNF@ZIF-8 solution. Notice the difference of colours between the CNF@ZIF-67 solutions.

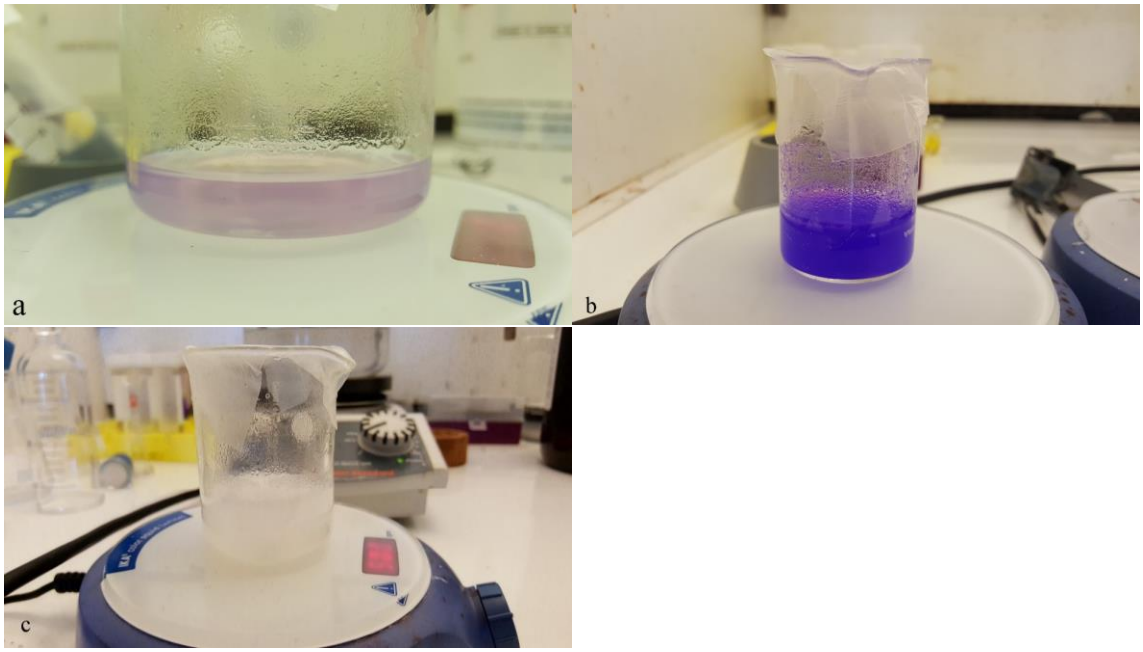

Figure F3. DTG curve of pure TEMPO-CNFs and CNF@ZIFs. First T_d of TEMPO-CNFs is marked with red, while for CNF@ZIF-67 in blue and CNF@ZIF-8 in magenta. Subsequent degradations in the nanocomposites are related to the ZIFs.